An investigation of Quantum Field Theories using Monte Carlo Simulations

Will Fletcher

Abstract: In this paper I aim to provide an introduction to Monte Carlo Simulations in general and then apply them to the study of the one dimensional harmonic oscillator and to the study of the free scalar field and the Sinh-Gordon and Sin-Gordon fields in two dimensions. Numerical results are compared to theoretical predictions and discussed.

Acknowledgements: I would like to thank Dr. Watts for all his guidance and advice, without which this project would never have got off the ground.

Contents

1 Statistical Computer Simulations

1.1 Introduction

Lattice Field Theories[1] have many formal analogies with statistical systems used in the description of thermodynamical behaviour, and can be investigated by numerical methods known as Monte Carlo simulations.

Monte Carlo simulations have been comprehensively applied to the study of lattice field theories and several important results have been achieved. Some have demonstrated, albeit numerically, the validity of long standing theoretical conjectures, whilst some have allowed the determination of interesting physical observables.

1.2 Formulation of a quantized lattice field system

Consider a Quantum Field Theory defined through the following formal steps:

1. Time is rotated to the imaginary axis, so as to achieve a positive definite Euclidean Metric in space-time.

2. A suitable action functional $S(\phi, m)$ of the field configuration is defined, where ϕ denotes the collection of all fields and m for all masses and other particle parameters of the theory.

3. For any observable $O(\phi)$ it's quantum expectation value is defined by averaging the value it takes on a given field configuration over all the field configurations with measure proportional to exp(-S), where we have adopted units $\hbar = c = 1$

$$< O >= Z^{-1} \int D\phi \; O(\phi) e^{-S(\phi,m)} \quad , \quad Z = \int D\phi \; e^{-S(\phi,m)}$$

The quantity Z is the vacuum to vacuum permanence amplitude, sometimes referred to as the partition function because of the analogy with the statistical formulation of a thermodynamical system. The quantum averages of $< O >$ are continued back, if necessary, to Minkowskian space-time.

What do the expressions above mean mathematically? The space-time continuum is replaced by the vertices of a lattice and the functional integrals above turn into ordinary multiple integrals by limiting the lattice to a finite volume V and defining the fields only at the lattice sites. The partial derivatives occuring in the kinetic part of S are also replaced with finite difference expressions. We can recover theoretical results through the thermodynamical limit $V \to \infty$ and the continuum limit $a \to 0$. The lattice regularized quantum expectation values are then given by:

$$< O >= Z^{-1} \int \prod_{xy} D\phi_{xy} \; O(\phi_{xy}) e^{-S(\phi_{xy},m)} \quad , \quad Z = \int \prod_{xy} D\phi_{xy} \; e^{-S(\phi_{xy},m)}$$

[1] are field theories formulated on a discrete lattice of points in Euclidean space-time.

1.3 Monte Carlo Estimation - A simple example

Monte Carlo simulations are the name collectively given to types of simulation that explicitly depend on (pseudo)random numbers. The name is derived from the famous Monaco casino, and emphasizes the importance of randomness in this method. As a quick example, I outline below a method for numerically determining the value of π by Monte Carlo estimation.

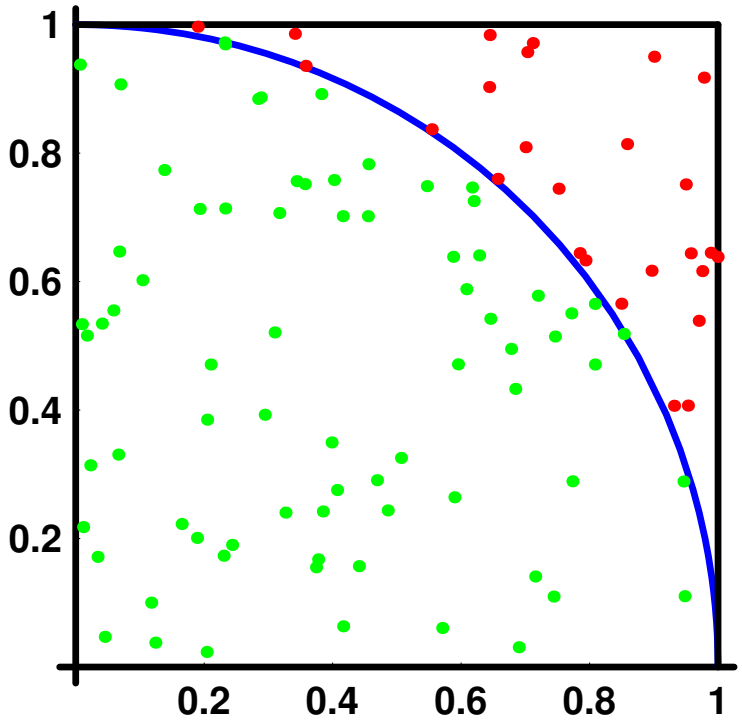

Figure 1: An example with 100 random points

The area of a circle is given by πr^2. So the area of one quarter of a unit circle is $n = \frac{1}{4}\pi$. That gives us $4n = \pi$. So by estimating the area of a quarter circle we can estimate the value of π. So the simulation takes the following steps:

1. Set two variables to zero, $M = N = 0$.
2. Pick a pair of random numbers, say a and b, both between 0 and 1.
3. $M = M + 1$ and if $a^2 + b^2 \leq 1$ then $N = N + 1$.
4. Repeat steps 2 and 3 a large number of times.
5. $\frac{N}{M}$ is an estimation of the area of the quarter circle.
6. so $\frac{4N}{M}$ is an estimation of π.

Every point is going to be within the unit square, that is why M is increased every time. Not every point will be within the unit circle quadrant. In the picture on the last page M is the number of green points and N is the number of green and red points. Increasing the number of random points chosen increases the accuracy of the estimate. For $M = 1000$ a quick simulation yielded the result $\pi_{estimate} = 3.142$. Although this is accurate, the process of Monte Carlo integration by this method becomes less accurate in situations involving integrals such as those at the end of section 1.2. A better solution is to use the process known as "importance sampling".

1.4 Importance Sampling

How do we evaluate the averages laid out at the end of the section 1.2? They could be (crudely) worked out by Monte Carlo estimation of the two integrals, perhaps using the same set of random numbers for evaluation of both integrals. However, this is not practical as a significant part of both integrals will tend to be concentrated in a small region of the phase-space due to the exponential factor.

If the phase space is discrete so that the action $S(\phi, m)$ is also discrete, i.e. $S = \sum_k S_k \ = \sum_k S(\phi_k, m)$ then the integrals turn into summations over the discrete states S_k.

$$< O >= Z^{-1} \sum_k O(\phi_k)\ e^{-S(\phi_k,m)} \qquad , \qquad Z = \sum_k\ e^{-S(\phi_k,m)}$$

It is impractical, and in most cases near impossible, to perform these sums over all possible configurations. So we can obtain an estimate by summing k over a finite subset of M configurations. Clearly, the representativeness of the subset and the size of M will affect the accuracy of the calculated estimate. This is where importance sampling plays a key role. The idea is to choose our M configurations in some way that is biased in favour of configurations of the form we desire. If the probability of a certain configuration ϕ_k appearing in the sample of representative configurations is given by $P(\phi_k)$ then the sums become:

$$< O >= Z^{-1} \sum_{k=1}^{M} \frac{O(\phi_k)\ e^{-S(\phi_k,m)}}{P(\phi_k)} \qquad , \qquad Z = \sum_{k=1}^{M} \frac{e^{-S(\phi_k,m)}}{P(\phi_k)}$$

Of interest, in this paper, are configurations chosen with the probability $P(\phi_k) \propto e^{-S(\phi_k,m)}$, then the so called Boltzmann factors will cancel out and the average, summed over M configurations, simply becomes:

$$< O >= M^{-1} \sum_{k=1}^{M} O(\phi_k)$$

This is a calculation that is much less labour (or CPU) intensive. The problem then becomes how to choose our configurations in such a manner that this labour saving process can be applied. The answer is to use the Metropolis Algorithm.

1.5 The Metropolis Algorithm

Configurations with the convenient property outlined in the last section can be generated by means of the Metropolis Algorithm. To reiterate, the Metropolis Algorithm allows us to create a sample of representative configurations, where the probability of a certain configuration occurring is directly proportional to that configuration's Boltzmann factor. Since first proposed[2] it has become both important and widespread in the realm of the Monte Carlo method.

Given a configuration ϕ_k and a transition probability function $T(\phi_k \rightarrow \phi_{k+1})$, the Metropolis Algorithm constructs a new configuration ϕ_{k+1} from the one before by updating one variable of the configuration and calculating the change in the action. To make a sequence of such configurations, known as a Markov chain, approach a desired distribution it is sufficient (but not necessary) to impose a condition known as "detailed balance". If $P(\phi_k) = \frac{e^{S(\phi_k,m)}}{Z}$ is the probability of configuration ϕ_k, then detailed balance states that, for an arbitrary pair of configurations, the following equality should hold :

$$P(\phi_j)T(\phi_j \rightarrow \phi_k) = P(\phi_k)T(\phi_k \rightarrow \phi_j)$$

$$\Rightarrow \text{ If } T(\phi_k \rightarrow \phi_j) = 0 \text{ then } T(\phi_j \rightarrow \phi_k) = 0$$

$$\text{and if } T(\phi_k \rightarrow \phi_j) \neq 0 \Rightarrow \frac{T(\phi_k \rightarrow \phi_j)}{T(\phi_j \rightarrow \phi_k)} = \exp(-\delta S) \quad \text{where } \delta S = S_j - S_k$$

This last equation implies that a move from one configuration to another is only possible if the inverse move is also possible. In light of this, the Metropolis Algorithm proceeds thus:

1. A proposed new lattice site value r is chosen randomly from a particular probability distribution.
2. The change in δS from replacing a lattice site ϕ_k by r is calculated.
3. The new site value r is accepted with probability $P_{accept} = \text{Min}(1, e^{-\delta S})$.

Steps 1 to 3 are repeated systematically on each lattice site in turn until the entire lattice has been covered[3]. Infact, step 3 can be expanded into a number of "substeps" to make the process more efficient for the computer. They are detailed below to provide a better explanation of what is happening.

1. If $\delta S < 0$ the new site value r is accepted.
2. If not, a random number R is chosen uniformly from the interval [0,1].
3. The new site value r is accepted if $e^{-\delta S} > R$.
4. Otherwise the lattice site remains unchanged.

[2] by Metropolis et al. in 1953

[3] This is referred to as one "sweep" of the lattice.

1.6 Putting it all together

There are many other aspects and matters of simulation fine tuning that need to be taken into account, such as how to discretize the action. Before discussing these finer points, I shall quickly lay out the steps involved in a Monte Carlo simulation.

1. An initial lattice configuration is chosen.
2. A certain number of sweeps are performed to thermalize the system.
3. The current configuration or calculations based on it are stored for later inspection.
4. A number of further sweeps are performed to decorrelate the current lattice configuration from the last stored one.
5. Steps 3 and 4 are repeated a large number of times.
6. Once finished, the stored configurations or the calculations based on them are analysed and averaged to provide a reliable estimate of the physical observables that one is seeking.

The initial configuration can be what is known as a "hot start", where the lattice site values are chosen randomly from some probability distribution, or a "cold start" where all the lattice site values are initially set to be constant and equal, normally to zero. A large number of thermalisation sweeps have to be performed in order to transform the hot or cold start into a lattice configuration that matches the desired canonical probability distribution.

A couple of fine tuning issues remain. Firstly, it is desirable for the Metropolis Algorithm to change a site's value roughly 50% of the time. This is because if the acceptance rate is too high, then the simulation moves through the phase space too slowly, and if the acceptance rate is too low then a lot of time is wasted on rejections. An acceptance rate that is very close to 50% is easily achieved by fine tuning a single parameter that decides how the random number r from the last page is chosen. Choosing the proposed site update r from a normal distribution, that is centred on the old site value ϕ_k, allows one to fine tune the acceptance rate by choosing different values of the variance σ and observing the effect.

Another issue to be considered is how to choose how many sweeps to perform in step 4 above. This is decided by measuring something that is known as the autocorrelation, which shall be explained in a later section. This fine tuning process, once again, is crucial to both the accuracy and efficiency of the Monte Carlo simulation. If too few a number of sweeps are ignored between stored configurations, then the configurations won't be sufficiently decorrelated from each other and any calculations based on those configurations will be inaccurate at best. If too many configurations are ignored, the calculations will be accurate but the simulation will take longer than necessary.

1.7 The Autocorrelation Function and Decorrelation

A quick calculation shows that for a 32×32 lattice, where 5000 configurations are stored for calculations and 200 sweeps are performed between each stored calculation we have to perform the Metropolis Algorithm a total of:

$$32 \times 32 \times 200 \times 5000 \approx 10^9 \quad \text{times!}$$

Clearly, this is a huge number of calculations and so any extra speed that can be squeezed out of the simulation by fine tuning the acceptance rate is most welcome. As previously mentioned, another way to increase the efficiency of the simulation and something that is absolutely crucial to it's accuracy is the number of sweeps to perform between stored, or calculation, configurations. This is decided by means of the autocorrelation function. Given a sequence of configurations $(\phi(1), \phi(2), \cdots)$ it is defined as:

$$ac(T) \;=\; \frac{1}{N}\sum_{k=1}^{N}\left(\sum_{i,j=1}^{M}\phi_{ij}(k)\phi_{ij}(k+T)\right)$$

The subscripts i and j denote two dimensional lattice coordinates and the subscript k denotes the position of the configuration ϕ in the sequence of stored configurations. M is the size of the lattice, and N is the number of different starting positions that the autocorrelation function is averaged over.

The purpose of averaging the autocorrelation in this manner is to smooth out statistical variations in the different configurations. The graph below and the two on the next page show a sample autocorrelation function worked out and averaged over 100, 1000 and then 10000 different starting positions.

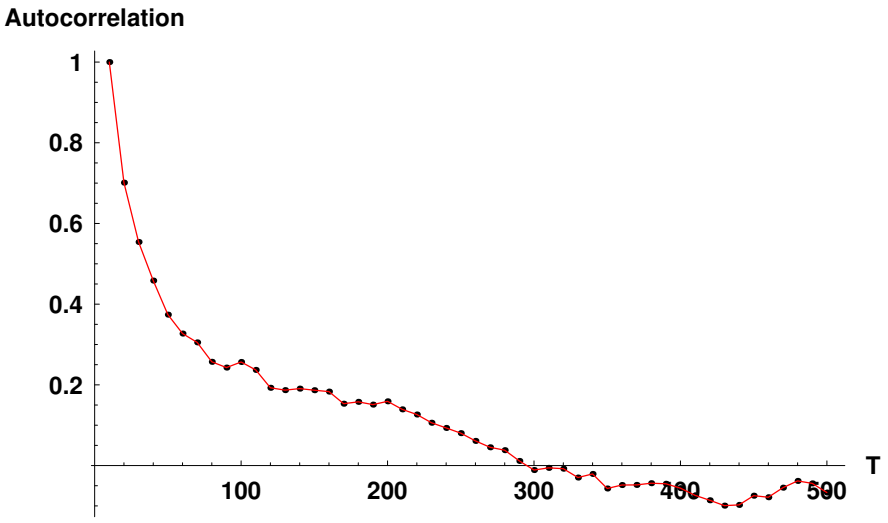

Figure 2: Averaged over 100 different starting positions.

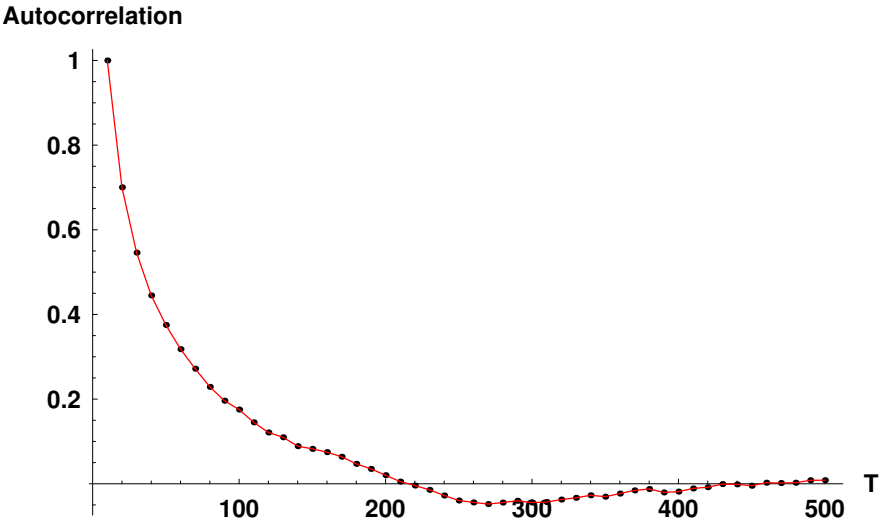

Figure 3: Averaged over 1,000 different starting positions.

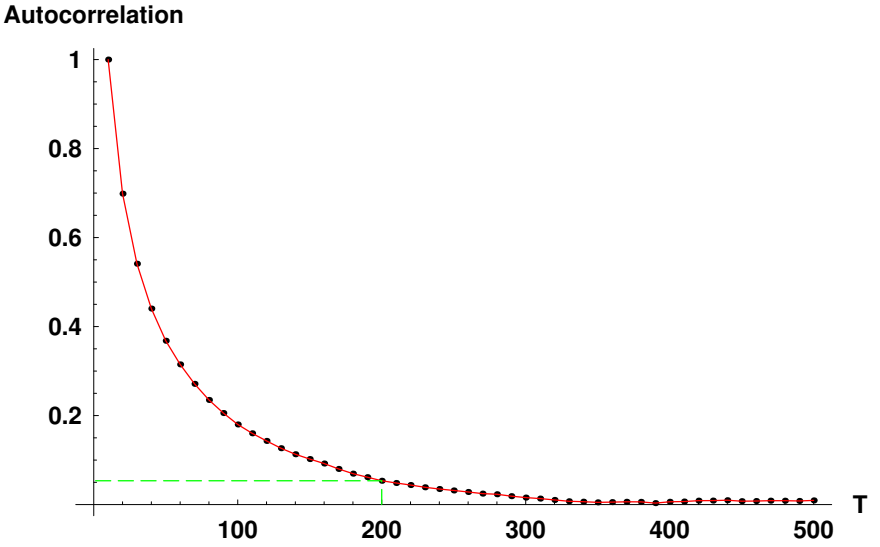

Figure 4: Averaged over 10,000 different starting positions.

In this case, which shall later be referred to as Case 7, performing 200 lattice sweeps between configurations used for calculations would be suitable. If less intermediate sweeps were performed, the autocorrelation value would be too high, whilst if more intermediate sweeps were performed, the simulation would take significantly longer for little or no gain in accuracy.

2 My simulations

2.1 Discretizing the Action

I now plan to elaborate on the previous section, and explain how it applies to the simulations I have carried out. First I shall explain briefly what the action $S(\phi, m)$ is and how it is discretized. Classically:

$$S = \int dt\ L\left(x, \frac{dx}{dt}\right)$$

This is just the time integral of the Lagrangian, where the Lagrangian of a system is equal to the system's kinetic energy minus the system's potential energy, i.e. $L = T - V$.

Now $V = V(\phi)$ is easy to discretize. One simply replaces, the continuous variable ϕ with the discrete variable ϕ_k in one dimension, or with the discrete variable ϕ_{xy} in two dimensions. So the discretized potential is simply $V = V(\phi_k)$ or $V = V(\phi_{xy})$.

The kinetic energy is more difficult to discretize as it contains derivatives of ϕ rather than containing ϕ explicitly. The kinetic energy term always has the basic form $\partial^\mu \phi\ \partial_\mu \phi$ or simply $(\partial_\mu \phi)^2$ in Euclidean space-time as covariant and contravariant indices mean the same thing. So, if D is the number of spatial dimensions, the discretized action has the form:

$$S = \int dt \left(\sum_{\mu=1}^{D} \frac{1}{2} (\partial_\mu \phi_k)^2 \ + \ V(\phi_k) \right)$$

Discretization of derivatives can be performed in many ways. A simple method would be to replace each of the first derivatives in the kinetic term with a discrete counterpart, the simplest being known as the forward and back derivatives.

$$(\partial_\mu \phi_k)^2 \to (\phi_{k+1} - \phi_k)^2 \quad \text{or} \quad (\partial_\mu \phi_k)^2 \to (\phi_k - \phi_{k-1})^2$$

Although the discretization scheme chosen should not effect the value of physical observables calculated in the simulation, the preferred method makes use of a second order derivative approximation known as the central difference method. Firsty, we can rewrite the derivative term:

$$(\partial_\mu \phi_k)^2 \ = \ \partial_\mu \phi_k\ \partial_\mu \phi_k \ = \ -\phi_k\ \partial_\mu^2 \phi_k \quad \text{by partial integration.}$$

The central difference approximation gives: $\partial^2 \phi_k \ = \ (\phi_{k+1} + \phi_{k-1} - 2\,\phi_k)$

This is fine for one dimension, but in 2 dimensions we have to remember that there is a second derivative in each of two directions. Taking this into account the kinetic term in two dimensions becomes:

$$\partial^2 \phi_{xy} \ = \ (\phi_{x,y+1} \ + \ \phi_{x,y-1} \ + \ \phi_{x+1,y} \ + \ \phi_{x-1,y} \ - \ 4\ \phi_{xy})$$

The final step in discretization is to replace the integral over time in the action with a sum over discrete variables. i.e. $\int dt \rightarrow \sum_k$. So the final form of the discretized action, in one and two dimensions respectively, becomes:

$$S = \sum_k \left[-\frac{1}{2}\, \phi_k(\phi_{k+1} + \phi_{k-1} - 2\,\phi_k) + V(\phi_k) \right]$$

$$S = \sum_{xy} \left[-\frac{1}{2}\, \phi_{xy}(\phi_{x,y+1} + \phi_{x,y-1} + \phi_{x+1,y} + \phi_{x-1,y} - 4\,\phi_{xy}) + V(\phi_{xy}) \right]$$

To save space we can denote the surrounding terms $S_1(k) = \phi_{k+1} + \phi_{k-1}$ and $S_2(xy) = \phi_{x,y+1} + \phi_{x,y-1} + \phi_{x+1,y} + \phi_{x-1,y}$ to get:

$$S = \sum_k \left[-\frac{1}{2}\, \phi_k(S_1(k) - 2\,\phi_k) + V(\phi_k) \right]$$

$$S = \sum_{xy} \left[-\frac{1}{2}\, \phi_{xy}(S_2(xy) - 4\,\phi_{xy}) + V(\phi_{xy}) \right]$$

Before proceeding, it is necessary to include the explicit form of the potentials in the action. The potentials for the scenarios I have been simulating are as follows:

$$V_1(\phi) = \frac{1}{2}\omega^2\phi^2 \qquad \text{for the one dimensional harmonic oscillator.}$$

$$V_2(\phi) = \frac{1}{2}m^2\phi^2 \qquad \text{for the two dimensional free scalar field.}$$

$$V_3(\phi) = \frac{m^2}{\beta^2}[1 - \cosh(\phi)] \qquad \text{for the sinh-gordon field in two dimensions.}$$

$$V_4(\phi) = \frac{m^2}{\beta^2}[\cos(\phi) - 1] \qquad \text{for the sin-gordon field in two dimensions.}$$

We can also introduce a lattice spacing constant a. The continuum limit is represented by $a \rightarrow 0$ and taking different values of a corresponds to rescaling the lattice. So including the lattice spacing a, and the explicit form of the potentials $V_i(\phi)$ into the four actions gives:

$$S_1 = \sum_{k=1}^{N} \left[-\frac{1}{2a}\, \phi_k[S_1(k) - 2\,\phi_k] + \frac{a}{2}\omega^2\phi_k^2 \right]$$

$$S_2 = \sum_{x,y=1}^{N} \left[-\frac{1}{2a}\, \phi_{xy}[S_2(xy) - 4\,\phi_{xy}] + \frac{a}{2}m^2\phi_{xy}^2 \right]$$

$$S_3 = \sum_{x,y=1}^{N} \left[-\frac{1}{2a}\, \phi_{xy}[S_2(xy) - 4\,\phi_{xy}] + \frac{a\,m^2}{\beta^2}[1 - \cosh(\phi_{xy})] \right]$$

$$S_4 = \sum_{x,y=1}^{N} \left[-\frac{1}{2a}\, \phi_{xy}[S_2(xy) - 4\,\phi_{xy}] + \frac{a\,m^2}{\beta^2}[\cos(\phi_{xy}) - 1] \right]$$

The similarity between S_1 and S_2 is unsurprising, the free scalar field is just a collection of harmonic oscillators, which are coupled by the gradient term $\partial_j\phi\ \partial_j\phi$ in the action or Hamiltonian.

The process does not stop here however. In the simulation we are interested in the change to the action caused by replacing one of the ϕ_k or ϕ_{xy} with a new value, r say. It would be extremely inefficient and impractical to calculate the whole sum every time the Metropolis Algorithm analysed a proposed site update. For a particular site ϕ_k or ϕ_{xy} the explicit changes in the action are given by:

$$\begin{aligned}
\delta S_1 &= (\phi_k - r)\left[\frac{S_1(k)}{a} - (\phi_k + r)\left(\frac{1}{a} + \frac{a}{2}\omega^2\right)\right] \\
\delta S_2 &= (\phi_{xy} - r)\left[\frac{S_2(xy)}{a} - (\phi_{xy} + r)\left(\frac{2}{a} + \frac{a}{2}m^2\right)\right] \\
\delta S_3 &= \frac{1}{a}(\phi_{xy} - r)\left[S_2(xy) - 2\,(\phi_{xy} + r)\right] + \frac{a\ m^2}{\beta^2}\left[\cos(\beta\phi_{xy}) - \cos(\beta r)\right] \\
\delta S_4 &= \frac{1}{a}(\phi_{xy} - r)\left[S_2(xy) - 2\,(\phi_{xy} + r)\right] + \frac{a\ m^2}{\beta^2}\left[\cosh(\beta r) - \cosh(\beta\phi_{xy})\right]
\end{aligned}$$

It is these changes to the action that the Metropolis Algorithm evaluates. Structuring them in this manner, so as to perform as few multiplications as possible is a further effort to speed up the simulation. In general multiplications take more CPU time than additions.

2.2 The actual simulation process

Many simulations were performed, over a wide variety of values for the input parameter values, in all four regimes. For each simulation I chose a cold start on the lattice. After 1000 thermalisation sweeps, a further 10,100 sweeps would be performed for the purposes of analysing the acceptance ratio and decorrelation length. After experimentation with each scenario, the optimum value of the variance σ and the minimum number of sweeps to perform between calculations were determined and the simulation could begin in earnest.

With the fine tuned parameters, the program would be run again in the manner laid out in previous sections. The next few sections will discuss and prove many theoretical results from the four regimes mentioned above. Following that will be another section containing comment and discussion on the simulation results found and comparing them to the theoretical predictions. Tables of simulation parameters and results, as well as graphs of relevant functions are included in Appendix A and B respectively, at the end of the paper.

3 One Dimensional Theory

3.1 nth roots of unity

The following result also applies to two dimensional theory. Consider $\omega = e^{\frac{2\pi i}{N}}$

$$\text{If } j \neq l : \sum_{k=0}^{N-1} \frac{(\omega^{(l-j)})^k}{N} = \frac{1}{N}(1+\omega^{(l-j)}+\omega^{2(l-j)}+\cdots+\omega^{(N-1)(l-j)}) = \frac{1}{N}\frac{1-(\omega^{(l-j)})^N}{1-\omega^{(l-j)}} = 0$$

Clearly if $j = l$ the sum equals 1 hence we have: $\sum_{k=0}^{N-1} \frac{(\omega^{(l-j)})^k}{N} = \delta_{lj}$

3.2 Fourier Transform of the lattice sites

The Fourier Transform p_j of the variable x_k in momentum space is defined by

$$p_j = \sum_{k=0}^{N-1} \frac{\omega^{jk}}{\sqrt{N}} x_k \qquad \text{and} \qquad x_j = \sum_{k=0}^{N-1} \frac{\omega^{-jk}}{\sqrt{N}} p_k \text{ where } \omega = e^{\frac{2\pi i}{N}}$$

$$\Rightarrow x_j = \sum_{k=0}^{N-1} \frac{\omega^{-jk}}{\sqrt{N}} \frac{\omega^{kl}}{\sqrt{N}} x_l = \sum_{k=0}^{N-1} \frac{\omega^{k(l-j)}}{N} x_l = \left(\sum_{k=0}^{N-1} \frac{(\omega^{(l-j)})^k}{N} \right) x_l = \delta_{lj}\, x_l = x_j$$

3.3 Fourier Transform of the lattice action

We shall now consider the discrete action for the Simple Harmonic Oscillator in one dimension on a periodic lattice with boundary condition $x_0 = x_N$:

$$\begin{aligned}
S &= \sum_{l=0}^{N-1} A{x_l}^2 + Bx_l x_{l+1} \quad \text{where } A = \frac{1}{2}\, am^2 + \frac{1}{a} \text{ and } B = -\frac{1}{a} \\
&= \sum_{j,\ k,\ l=0}^{N-1} A\frac{\omega^{lj}\omega^{lk}}{N} p_j p_k + B\frac{\omega^{lj}\omega^{(l+1)k}}{N} p_j p_k \\
&= \sum_{j,\ k=0}^{N-1} \left(\sum_{l=0}^{N-1} \frac{\omega^{l(j+k)}}{N} \right) (A + B\omega^k) p_j p_k = \sum_{j,\ k=0}^{N-1} \delta_{j,-k}(A + B\omega^k) p_j p_k \\
&= \sum_{k=1}^{\frac{N}{2}-1} \{2A + B(\omega^k + \omega^{-k})\} p_k p_{-k} = \sum_{k=1}^{\frac{N}{2}-1} \{2A + 2B\cos(\frac{2\pi k}{N})\} p_k p_{-k} \\
&= \sum_{v,w=1}^{\frac{N}{2}-1} S_{vw} p_v p_w \quad \text{where } S_{vw} = S_w\ \delta_{v,-w} \ = \ \{2A + 2B\cos(\frac{2\pi w}{N})\}\delta_{v,-w}
\end{aligned}$$

3.4 Calculation of the correlation function propagator

$$< x_1 \cdots x_n > = \frac{1}{Z} \int Dx\, e^S\, x_1 \cdots x_n = \left(\frac{\partial}{\partial t_1} \cdots \frac{\partial}{\partial t_n} \int Dx\ e^{\,S\, +\, t_1 x_1\, +\, \cdots\, +\, t_n x_n} \right) \Big|_{\,t_i = 0}$$

where $Dx = \prod_x dx$ and S is the discrete lattice action described in the last section.

Z is a normalisation constant chosen such that $< 1 > = 1$. In other words $\Rightarrow Z = \int Dx\, e^S$

$$\begin{aligned}
\Rightarrow < p_1 \cdots p_n > &= \frac{1}{Z} \int Dp\, e^S\, p_1 \cdots p_n \\
&= \left(\frac{\partial}{\partial q_1} \cdots \frac{\partial}{\partial q_n} \int Dx\ e^{\,S\, +\, q_1\ p_1\, +\, \cdots\, +\, q_n\ p_n} \right) \Big|_{\,q_i = 0} \\
&= \left(\frac{\partial}{\partial q_1} \cdots \frac{\partial}{\partial q_n}\ < \sum_{m=1}^{n} q_k p_k > \right) \Big|_{\,q_i = 0} \\
&= \left(\frac{\partial}{\partial q_1} \cdots \frac{\partial}{\partial q_n}\ Q \right) \Big|_{\,q_i = 0} \\
&= \frac{\partial}{\partial q_1} \cdots \frac{\partial}{\partial q_n}\ \exp \left(\sum_{k=0}^{N-1} \frac{q_k q_{-k}}{2A + 2B\cos(\frac{2\pi k}{N})} \right) \Big|_{\,q_i = 0}
\end{aligned}$$

The last line was reached through the change of variables $p_{\pm k} \rightarrow p_{\pm k} - \frac{q_{\mp k}}{2A + 2B\cos(\frac{2\pi k}{N})}$ as

$$\begin{aligned}
Q &= \frac{1}{Z} \int \prod dp\ \exp\ (\sum_{k=0}^{N-1} p_k p_{-k} \{2A + 2B\cos(\frac{2\pi k}{N})\} + p_k q_k + p_{-k} q_{-k}) \\
&= \frac{1}{Z} \prod \left(\int dp_k\ dp_{-k}\ \exp\ (p_k p_{-k} \{2A + 2B\cos(\frac{2\pi k}{N})\} + p_k q_k + p_{-k} q_{-k} \right) \\
&= \frac{1}{Z} \prod \left(\int dp_k\ dp_{-k}\ \exp\ \left(p_k p_{-k} \{2A + 2B\cos(\frac{2\pi k}{N})\} + \frac{q_k q_{-k}}{2A + 2B\cos(\frac{2\pi k}{N})} \right) \right) \\
&= \left\{ \frac{1}{Z} \int \prod dp\ \exp\ \left(\sum_{k=0}^{N-1} p_k p_{-k} \{2A + 2B\cos(\frac{2\pi k}{N})\} \right) \right\} \left\{ \exp \left(\sum_{k=0}^{N-1}\ \frac{q_k q_{-k}}{2A + 2B\cos(\frac{2\pi k}{N})} \right) \right\} \\
&= \prod \exp \left(\frac{q_k q_{-k}}{2A + 2B\cos(\frac{2\pi k}{N})} \right)\ = \exp\ \left(\sum_{k=0}^{N-1} \frac{q_k q_{-k}}{2A + 2B\cos(\frac{2\pi k}{N})} \right)
\end{aligned}$$

$$\Rightarrow < p_j p_{-k} > = G_k\, \delta_{jk} \ \text{ where } \ G_k\ = \frac{1}{2A + 2B\cos(\frac{2\pi k}{N})}$$

3.5 Expectation Values

Using $< x_j x_k > = \sum_{m,n=0}^{N-1} \frac{\omega^{jm}\omega^{kn}}{N} < p_m p_n >$ and 1.1 we can calculate expectation values.

Since $< p_m p_{-n} > = G_m\, \delta_{mn}$ we have $< x_j x_k > = \frac{1}{N} \sum_{m=0}^{N-1} \omega^{m(j-k)} < p_m p_{-m} >$

$$\Rightarrow < x_j\, x_k > = \frac{1}{N} \sum_{m=0}^{N-1} \omega^{m(j-k)} G_m \text{ so if } j = k \text{ we have } < x_j\, x_j > = \frac{1}{N} \sum_{m=0}^{N-1} G_m$$

$$\Rightarrow N < x^2 > = \sum_{k=0}^{N-1} \frac{1}{2A + 2B\cos(\frac{2\pi k}{N})} = \frac{1}{2A+2B} + \frac{1}{2A-2B} + \sum_{k=1}^{N/2-1} \frac{1}{A + B\cos(\frac{2\pi k}{N})}$$

Notice that, without ambiguity or loss of generality, we can write $< x^2 >$ above as the index j does not appear explicitly on the right hand side.

For the one-dimensional harmonic oscillator we had $A = \frac{1}{2}\, am^2 + \frac{1}{a}$ and $B = -\frac{1}{a}$

$$\Rightarrow < x^2 > = \frac{1}{N} \left(\frac{1}{a\, m^2} + \frac{a}{2 + a^2 m^2} + \sum_{k=1}^{N/2-1} \frac{2}{a\, m^2 + \frac{2}{a}\{1 - \cos(\frac{2\pi k}{N})\}} \right)$$

4 Two Dimensional Theory

4.1 Fourier Transform of the lattice sites

The Fourier Transform p_{jk} of x_{mn} in momentum space is defined by

$$p_{jk} = \sum_{m,n=0}^{N-1} \frac{\omega^{jm}\omega^{kn}}{N} x_{mn} \qquad \text{and} \qquad x_{jk} = \sum_{j,k=0}^{N-1} \frac{\omega^{-jm}\omega^{-kn}}{N} p_{mn} \text{ where } \omega = e^{\frac{2\pi i}{N}}$$

$$\Rightarrow\ x_{jk} = \sum_{m,n,r,s=0}^{N-1} \frac{\omega^{-(jm+kn)}}{N}\frac{\omega^{mr+ns}}{N} x_{rs} = \sum_{r,s=0}^{N-1} \left(\sum_{m=0}^{N-1} \frac{\omega^{m(r-j)}}{N}\right)\left(\sum_{n=0}^{N-1} \frac{\omega^{n(s-j)}}{N}\right) x_{rs}$$

Using the results of 1.1 we find that, as one would expect: $x_{jk} = \delta_{rj}\,\delta_{sk}\,x_{rs} = x_{jk}$

4.2 Fourier Transform of the lattice action

We shall now consider the discrete action for the free scalar field in two dimensions on a periodic lattice with boundary conditions $x_{j0} = x_{jN}$ and $x_{0k} = x_{Nk}$

$$S = \sum_{u,v=0}^{N-1} A\,x_{uv}^2 + B\,(x_{uv}x_{uv+1} + x_{uv}x_{u+1v}) \text{ where } A = \frac{1}{2}\,am^2 + \frac{2}{a} \text{ and } B = -\frac{1}{a}$$

$$\begin{aligned}
\text{Now } \sum_{u,v=0}^{N-1} A\,x_{uv}^2 &= \sum_{u,v,m,n,r,s=0}^{N-1} A\,\frac{\omega^{-u(r+m)}}{N}\frac{\omega^{-v(s+n)}}{N} p_{mn}p_{rs} \\
&= \sum_{m,n,r,s=0}^{N-1} A\left\{\left(\sum_{u=0}^{N-1}\frac{\omega^{-u(r+m)}}{N}\right)\left(\sum_{v=0}^{N-1}\frac{\omega^{-v(s+n)}}{N}\right) p_{mn}p_{rs}\right\} \\
&= \sum_{m,n,r,s=0}^{N-1} A\,\delta_{r,-m}\,\delta_{s,-n}\,p_{mn}p_{rs} = \sum_{r,s=0}^{N-1} A\,p_{r,s}p_{-r,-s}
\end{aligned}$$

$$\sum_{u,v=0}^{N-1} B\,x_{uv}x_{uv+1} = \sum_{r,s=0}^{N-1} B\,\omega^{-s}\,p_{r,s}p_{-r,-s} \qquad \text{and}$$

$$\sum_{u,v=0}^{N-1} B\,x_{uv}x_{u+1v} = \sum_{r,s=0}^{N-1} B\,\omega^{-r}\,p_{r,s}p_{-r,-s} \qquad \text{using the same method.}$$

So the transformed action is: $S = \sum_{r,s=0}^{N-1} \left(B\,\omega^{-s} + B\,\omega^{-r} + A\right)\,p_{rs}\,p_{-r,-s}$

$$\Rightarrow\ S = \sum_{r,s=1}^{N/2-1} S_{srfg}\ p_{sf}\,p_{rg} \text{ where } S_{srfg} = \left(2B\cos\frac{2\pi s}{N} + 2B\cos\frac{2\pi r}{N} + 2A\right)\delta_{s,-f}\,\delta_{r,-g}$$

4.3 Calculation of the correlation function propagator

We can calculate the propagator for the scalar field, using the same method as we did in section 3.4 for the harmonic oscillator, by introducing an external source to the partition function. It is, once again, the inverse of the lattice action, in this case S_{rsfg}. An outline for the calculation is provided below, but for brevity some of the intermediate steps are excluded.

$$< x_{i_1 j_1} \cdots x_{i_n j_n} > = \frac{1}{Z} \int Dx\, e^S\, x_{i_1 j_1} \cdots x_{i_n j_n} \text{ where } Dx = \prod_{ij} dx_{ij} \text{ and } Z = \int Dx\, e^S$$

$$\Rightarrow < p_{i_1 j_1} \cdots p_{i_n j_n} > = \frac{\partial}{\partial q_{i_1 j_1}} \cdots \frac{\partial}{\partial q_{i_n j_n}} \exp \left(\sum_{r,s=0}^{N-1} \frac{q_{rs} q_{-r,-s}}{2B \left(\cos \frac{2\pi s}{N} + \cos \frac{2\pi r}{N} \right) + 2A} \right) \Bigg|_{q_i = 0}$$

The result was again reached through evaluating $< \exp \left(\sum_{i,j=0}^{N-1} p_{ij} q_{ij} \right) >$ using a change of variables, in this case: $p_{\pm r, \pm s} \rightarrow p_{\pm r, \pm s} - \frac{q_{\mp r, \mp s}}{2B \left(\cos \frac{2\pi s}{N} + \cos \frac{2\pi r}{N} \right) + 2A}$

$$\Rightarrow < p_{rs} p_{-m,-n} > = G_{rs}\, \delta_{rm}\, \delta_{sn} \text{ where } G_{rs} = \frac{1}{2B \left(\cos \frac{2\pi s}{N} + \cos \frac{2\pi r}{N} \right) + 2A}$$

4.4 Expectation Values

Using $< x_{jk}\, x_{uv} > = \sum_{m,n,r,s=0}^{N-1} \frac{\omega^{jm} \omega^{kn}}{N} \frac{\omega^{ur} \omega^{vs}}{N} < p_{mn} p_{rs} >$ expectation values are calculated using: $< p_{rs} p_{-m,-n} > = G_{rs}\, \delta_{rm}\, \delta_{sn}$

$$\Rightarrow < x_{jk}\, x_{uv} > = \frac{1}{N^2} \sum_{m=0}^{N-1} \omega^{r(u-j)} \omega^{s(v-k)}\, G_{rs} \quad \Rightarrow < x_{jk}\, x_{jk} > = \frac{1}{N^2} \sum_{r,s=0}^{N-1} G_{r,s}$$

$$\Rightarrow < x^2 > = \frac{1}{N^2} \sum_{r,s=0}^{N-1} \frac{1}{2B \left(\cos \frac{2\pi s}{N} + \cos \frac{2\pi r}{N} \right) + 2A}$$

For the free scalar field in two dimensions: $A = \frac{1}{2} am^2 + \frac{2}{a}$ and $B = -\frac{1}{a}$

$$\Rightarrow < x^2 > = \frac{1}{N^2} \left(\sum_{r,s=0}^{N-1} \frac{a}{a^2 m^2 + 2 \left(2 - \cos \frac{2\pi s}{N} + \cos \frac{2\pi r}{N} \right)} \right)$$

5 Continuum results

5.1 One dimensional Harmonic Oscillator

The Lagrangian and Hamiltonian for a classical system with position x and velocity $\frac{dx}{dt}$ are given by the two equations below.

$$L = \frac{1}{2}\left(\frac{dx}{dt}\right)^2 - \frac{1}{2}\,\omega^2 x^2 \qquad \text{and} \qquad H = \frac{1}{2}p^2 + \omega^2 x^2$$

The creation and annihilation operators, denoted $\alpha^\dagger$ and α, are defined here as:

$$\alpha = \frac{\omega x + ip}{\sqrt{2\omega}} \quad \text{and} \quad \alpha^\dagger = \frac{\omega x - ip}{\sqrt{2\omega}} \quad \Rightarrow \quad x = \frac{\alpha + \alpha^\dagger}{\sqrt{2\omega}} \quad \text{and} \quad p = \sqrt{\frac{\omega}{2}}\frac{\alpha - \alpha^\dagger}{i}$$

Of course, the definitions of the creation and annihilation operators are just conventions, that may be defined in numerous ways. The similarity between the variety of possible definitions is that they satisfy certain commutation relations.

One such relation is $[\alpha,\alpha^\dagger] = 1$. We call $N = \alpha^\dagger\alpha$ the Number operator.

With the definitions above we find the Hamiltonian becomes: $H = \omega\left(N + \frac{1}{2}\right)$

and that x^2 transforms into: $x^2 = \frac{1}{2\omega}\left(\alpha^2 + \alpha\alpha^\dagger + \alpha^\dagger\alpha + \left(\alpha^\dagger\right)^2\right)$

Using Dirac notation $\alpha|n> = \sqrt{n}|n-1>$ and $\alpha^\dagger|n> = \sqrt{n+1}|n+1>$

Now $<n|\alpha^2|n> = 0$ and $<n|(\alpha^\dagger)^2|n> = 0$ since $<m|n> = \delta_{mn}$

$\Rightarrow 2\omega^2 <n|x^2|n> = <n|(\alpha\alpha^\dagger + \alpha^\dagger\alpha)|n> = <n|([\alpha,\alpha^\dagger] + 2\alpha^\dagger\alpha)|n>$

$\Rightarrow 2\omega^2 <n|x^2|n> = <n|(1+2N)|n> = 1 + 2n \Rightarrow <n|x^2|n> = \frac{1+2n}{2\omega}$

In the ground state with $n = 0$ we have $<0|x^2|0> = \frac{1}{2\omega}$ as one might expect.

5.2 One dimensional Harmonic Oscillator in Euclidean Time

In Euclidean Time a translation by T is generated by: $U(T) = e^{-TH}$

For a periodic system: $< O > = \mathrm{Tr}\, e^{-TH} O = \sum_n < n|e^{-TH}O|n >$

$$\Rightarrow < O > = \sum_n < n|O|n > e^{-(n+\frac{1}{2})\omega T} \quad \Rightarrow < x^2 > = \sum_n \left(\frac{1+2n}{2\omega}\right) e^{-n\omega T} e^{-\frac{\omega T}{2}}$$

$$\begin{aligned}
\Rightarrow < x^2 > &= \frac{e^{-\frac{\omega T}{2}}}{2\omega}\left(\sum_n e^{-n\omega T} + 2\sum_n n e^{-n\omega T}\right) = \frac{e^{-\frac{\omega T}{2}}}{2\omega}\left(\frac{1}{1-e^{-\omega T}} + \frac{2e^{-\omega T}}{(1-e^{-\omega T})^2}\right) \\
&= \frac{e^{-\frac{\omega T}{2}}}{2\omega}\left(\frac{1-e^{-\omega T}+2e^{-\omega T}}{(1-e^{-\omega T})^2}\right) = \frac{e^{-\frac{\omega T}{2}}}{2\omega}\left(\frac{1+e^{-\omega T}}{(1-e^{-\omega T})^2}\right) \\
&= \frac{1}{2\omega}\left(\frac{e^{\frac{\omega T}{2}}+e^{-\frac{\omega T}{2}}}{(e^{\frac{\omega T}{2}}+e^{-\frac{\omega T}{2}})^2}\right) = \frac{1}{2\omega}\left(\frac{2\cosh(\frac{\omega T}{2})}{\left(2\sinh\left(\frac{\omega T}{2}\right)\right)^2}\right) \\
&= \frac{1}{4\omega}\left(\frac{\coth(\frac{\omega T}{2})}{\sinh\left(\frac{\omega T}{2}\right)}\right)
\end{aligned}$$

Now $\sum_n < n|1|n > e^{-(n+\frac{1}{2})\omega T} = e^{-\frac{\omega T}{2}} \sum_n e^{-n\omega T} = \frac{e^{-\frac{\omega T}{2}}}{1-e^{-\omega T}} = \frac{1}{2\sinh(\frac{\omega T}{2})}$

So we are left with the normalised result: $\frac{< x^2 >}{< 1 >} = \frac{1}{2\omega}\coth\left(\frac{\omega T}{2}\right)$

As $T \to \infty$, $\coth\left(\frac{\omega T}{2}\right) \to 1$ and we regain the result for an infinite system.

6 Calculation of the Propagator in infinite space

6.1 The calcuation

In this section I shall calculate the propagator[4] $G(x-y)$ in infinite, Euclidean space. It is known that the operator $-\bigtriangledown^2 + m^2$ has $G(x-y)$ as it's Green's Function. Using a Fourier transform we can write:

$$G(x-y) \;=\; \int \frac{d^D p}{(2\pi)^D}\, G(p)\, e^{i\; p_\mu (x_\mu - y_\mu)} \quad \text{where} \quad G(p) \;=\; \frac{1}{p^2+m^2}$$

$$\text{Consider} \quad \frac{1}{A} \;=\; \frac{1}{2}\int_0^\infty d\alpha\; e^{-\frac{A}{2}\alpha} \quad \text{where} \;\; A>0 \;\; \text{is a positive real number.}$$

Using this identity, we can choose to take $A = p^2 + m^2$, and substitute this back into the integral expression for $G(x-y)$ given above.

$$\begin{aligned}
\Rightarrow G(x-y) \quad &= \quad \int \frac{d^D p}{(2\pi)^D}\, \frac{e^{i\; p_\mu (x_\mu - y_\mu)}}{p^2+m^2} \\
&= \quad \frac{1}{2}\int_0^\infty d\alpha \int \frac{d^D p}{(2\pi)^D}\; e^{-\frac{\alpha}{2}(p^2+m^2)+ip_\mu (x_\mu - y_\mu)} \\
&= \quad \frac{1}{2}\int_0^\infty d\alpha \int \frac{d^D p}{(2\pi)^D}\; e^{-\frac{1}{2}\left(\sqrt{\alpha}p_\mu - i\frac{x_\mu - y_\mu}{\sqrt{\alpha}}\right)^2 + \frac{1}{2}\left(\frac{x_\mu - y_\mu}{\sqrt{\alpha}}\right)^2 - \frac{m^2\alpha}{2}} \\
&= \quad \frac{1}{2}\int_0^\infty d\alpha\; e^{\frac{1}{2}\left(\frac{x_\mu - y_\mu}{\sqrt{\alpha}}\right)^2 - \frac{m^2\alpha}{2}} \left(\int \frac{d^D p}{(2\pi)^D}\; e^{-\frac{1}{2}\left(\sqrt{\alpha}p_\mu - i\frac{x_\mu - y_\mu}{\sqrt{\alpha}}\right)^2}\right) \\
&= \quad \frac{1}{2}\int_0^\infty d\alpha\; e^{\frac{1}{2}\left(\frac{x_\mu - y_\mu}{\sqrt{\alpha}}\right)^2 - \frac{m^2\alpha}{2}}\; (2\pi\alpha)^{-\frac{D}{2}} \\
&= \quad \frac{1}{2(2\pi)^{\frac{D}{2}}}\int_0^\infty d\alpha\; \alpha^{-\frac{D}{2}}\; e^{-\frac{|x-y|^2}{2\alpha} \; - \frac{m^2\alpha}{2}} \\
&= \quad \frac{1}{(2\pi)^{\frac{D}{2}}}\left(\frac{m}{|x-y|}\right)^{\frac{D}{2}-1}\; K_{\frac{D}{2}-1}\left(m\,|x-y|\right)
\end{aligned}$$

where the last line has been reached by the change of variables: $\alpha \;=\; \dfrac{|x-y|}{m}\, t$

$$\text{and} \;\; K_s(z) \;=\; \frac{1}{2}\int_0^\infty dt\; t^{s-1}\; e^{-\frac{z}{2}\left(t+\frac{1}{t}\right)} \;\; \text{where} \;\; s = \frac{D}{2} - 1 \;\; \text{and} \;\; z \;=\; m\,|x-y|$$

is the well-known integral representation of the Bessel function.

[4] otherwise known as the two-point correlation function

Now that we have an expression for the propagator, it's behaviour can be examined for different scenarios. Of particular interest are short distances where $z = m\,|x-y| \ll 1$ and long distances where $z = m\,|x-y| \gg 1$.

6.2 Short Distance behaviour

In this scenario $z \ll 1$. For small values of it's argument, the Bessel Function behaves as:

$$K_s(z) \approx \frac{\Gamma(s)}{(z/2)^2} + O\left(\frac{1}{z^{s-2}}\right)$$

$$\begin{aligned}
\Rightarrow G(x-y) &\approx \frac{\Gamma\left(\frac{D}{2}-1\right)}{4\pi^{\frac{D}{2}}\,|x-y|^{D-2}} \\
&\approx -\frac{1}{2\pi}\left(\mathrm{Log}\left[\frac{m|x-y|}{2}\right] - \gamma\right) && \text{if } D=2. \\
&\approx \frac{\Gamma(-1/2)\,|x-y|}{(4\pi)^{1/2}} = |x-y| && \text{if } D=1.
\end{aligned}$$

Above, γ represents a constant known as Euler's Constant and has the value $\gamma = 0.577216$. An interesting point here, is to note that the leading term is independent of the mass, in any number of dimensions[5]. So this expression represents the behaviour of the massless theory. Of more interest, and relevance to this paper, is:

6.3 Long Distance behaviour

In this scenario $z \gg 1$. A saddle point calculation indicates that the Bessel function $K_s(z)$ behaves asymptotically as:

$$K_s(z) \approx \sqrt{\frac{\pi}{2z}}\, e^{-z}\left[1 + O\left(\frac{1}{z}\right)\right]$$

$$\begin{aligned}
\Rightarrow G(x-y) &\approx \frac{\sqrt{\pi/2}\; m^{D-2} e^{-m|x-y|}}{(2\pi)^{\frac{D}{2}}\,(m|x-y|)^{\frac{D-1}{2}}}\left[1 + O\left(\frac{1}{m|x-y|}\right)\right] \\
&\approx \frac{1}{2\sqrt{2\pi}}\,\frac{e^{-m|x-y|}}{\sqrt{m|x-y|}} && \text{if } D=2. \\
&\approx \frac{1}{2m}\, e^{-m|x-y|} && \text{if } D=1.
\end{aligned}$$

So, at long distances, the Euclidean Green's Function decays exponentially. The correlation length can be seen to be $1/m$ which is unsurprising as it is the only variable in the theory with units of length.

[5] except the special case D=2.

7 Results and Discussion

7.1 One Dimensional Harmonic Oscillator

The results and the graphs for the Harmonic Oscillator are presented in Cases 1 to 6 in Appendix A and B respectively. The agreement between the expected and the computed values of the physical observables was very good, and likely to be due to the fact that the calculations were performed over 5000 configurations.

The value of $< x^2 >_{fit}$ matched the value of $< x^2 >_D$, that was calculated in Section 3.5, to within a very small margin of error, as can be seen in the results of section 10.1, and the exponential fit to the correlation function's long distance behaviour (that was calculated in Section 6.3) was also very accurate, as can be seen in Figures 5, 6 and 8.

The correlation function fit can be so accurate, even for small distances on the lattice, due to the lack of a $\frac{1}{\sqrt{x}}$ factor in it's long distance behaviour. This means that the correlation function "behaves well" for small distances, as can be seen in section 6.2.

Figure 7 shows a sample position probability distribution for the Harmonic Oscillator. The probability distribution was calculated by dividing the space axis into "bins" of equal width and counting how many lattice points fell into each bin. To get the good agreement shown in the figure it was necessary to average this probability distribution over many configurations. It was found, as expected, to be a Gaussian distribution, that is fitted in the figure by the function: $\sqrt{\frac{am}{\pi}}e^{-amx^2}$.

7.2 Two Dimensional Scalar Field

The results and the graphs for the Scalar Field are presented in Cases 7 to 12 in Appendix A and B respectively. The agreement between the expected and the computed values of the physical observables was, again, very good, and likely, once again, to be due to the fact that the calculations were performed over 5000 configurations.

The value of $< x^2 >_{fit}$ matched the value of $< x^2 >_D$, that was calculated in Section 4.4, to within a very small margin of error, as can be seen in the results of section 10.2, and the exponential fit to the correlation function's long distance behaviour (that was calculated in Section 6.3) was also very accurate, as can be seen in Figures 9 to 14.

The correlation function fit, due to the presence of a $\frac{1}{\sqrt{x}}$ factor in it's long distance approximation, "blows up" as $x \to 0$. This is why the long distance approximation does not agree with the numerical values that were calculated for the correlation function for small values.

The long distance behaviour of the correlation function, calculated in section 6.3, is theoretically predicted to begin being exhibited for distances longer than the correlation length $\left(\frac{1}{am}\right)$. This point is represented by the dashed lines in

figures 9 to 14 and, as can be seen in the graphs, theory and simulation do appear to match closely to the expected form after this point. The explicit match produced in figures 9 to 14 was producing by fitting the simulation data to $\sqrt{\frac{a}{2m}}\frac{e^{-amx}}{2\sqrt{x}}$, where a is the usual lattice spacing.

Figures 15 and 16 show probability distributions for the Scalar Field from cases 7 to 12. They were calculated in the same manner of "bin counting" and were once again found to be Gaussian.

7.3 Two Dimensional Sinh-Gordon Field

The results and the graphs for the Sinh-Gordon Field are presented in Cases 13 to 18 in Appendix A and B respectively. However, it cannot be assumed that the wavefunction is normalised correctly, so a mass renormalisation $m_{fit}(\beta)$ and a wavefunction normalisation $Z(\beta)$, where the correlation function takes the form $Z^2\frac{e^{-m(m_{fit})x}}{\sqrt{x}}$, was sought by the process of least square minimisation.

The process of least square minimisation simply involved finding the values of m_{fit} and Z that minimised:

$$\sum_x \left(< \phi(0)\ \phi(x) > \ - Z^2\frac{e^{-m(m_{fit})x}}{\sqrt{x}} \right)^2$$

In each case the calculations were averaged over 2500 configurations, $m = \frac{1}{2}$ was used and $a = 1$, which is why it does not explicitly appear in the above equation. Plots of the simulation correlation function data, compared to the expected form of the correlation function with the optimised value of m_{fit} are shown in figures 17 to 22.

The fit to the numerical correlation function data was very good, as can be seen in figures 17 to 22. Plotting m_{fit} against β^2 (figure 23) and calculating a line of best fit, indicates a linear relation between the mass renormalisation and the input parameter squared β^2. From this was deduced the approximate relation: $m_{fit} = 0.915882 + 0.100661\beta^2$.

Plotting $< \phi(0)^2 >$ against β^2 (figure 24) also seemed to indicate a linear relation which was deduced to be $< \phi(0)^2 > = 0.376131 - 0.0147825\beta^2$

The wavefunction normalisation constant was found to approximately follow the relation: $Z = 0.487644 - 0.00694171\beta^2$ as can be seen in figure 25.

7.4 Two Dimensional Sin-Gordon Field

The results and the graphs for the Sin-Gordon Field are presented in Cases 19 to 24 in Appendix A and B respectively. Mass and wavefunction renormalisation terms were calculated in the same manner as for the sinh-gordon field. In each case the calculations were averaged over 2500 configurations, $m = \frac{1}{2}$ was used as was $a = 1$.

Plots of the simulation correlation function data, compared to the expected form of the correlation function with the optimised value of m_{fit} are shown in figures 26 to 31.

The agreement between the fit and the simulation is again very good. Plotting m_{fit} against β^2 (figure 32) shows an approximate linear relation between the mass renormalisation and the input parameter squared β^2. From this was (tentatively) deduced the approximate relation: $m_{fit} = 0.919329 - 0.100169\beta^2$.

Plotting $< \phi(0)^2 >$ against β^2 (figure 33) also seemed to indicate a linear relation which was deduced to be $< \phi(0)^2 > = 0.37685 + 0.0164155\beta^2$.

The wavefunction normalisation constant was found to approximately follow the relation: $Z = 0.488345 + 0.00814477\beta^2$ as can be seen in figure 34.

7.5 Comparison of Sinh-Gordon and Sin-Gordon Results

The Sinh-Gordon field and Sin-Gordon field are related to each other by the transformation $\beta \to i\beta$, i.e. $\beta^2_{sinh} \to -\beta^2_{sin}$. It is pleasing then that we have:

$$\begin{aligned} < \phi(0)^2 >_{sinh} &= 0.376131 - 0.0147825\beta^2_{sinh} \\ &= 0.376131 + 0.0147825\beta^2_{sin} \\ &\approx 0.37685 + 0.0164155\beta^2_{sin} \\ &= < \phi(0)^2 >_{sin} \end{aligned}$$

and dropping the "fit" subscript from the mass renormalisation parameter in each case we have:

$$\begin{aligned} m_{sinh} &= 0.915882 + 0.100661\beta^2_{sinh} \\ &= 0.915882 - 0.100661\beta^2_{sin} \\ &\approx 0.919329 - 0.100169\beta^2_{sin} \\ &= m_{sin} \end{aligned}$$

This would indicate that the two sets of simulations (Cases 13 to 18 and Cases 19 to 24) although separate are infact complimentary. In other words:

$m_{sinh} \to m_{sin}$ and $< \phi(0)^2 >_{sinh} \to < \phi(0)^2 >_{sin}$ under $\beta^2_{sinh} \to -\beta^2_{sin}$

The fit found to the relation between the wavefunction normalisation constant Z, followed a similar relation:

$$\begin{aligned} Z_{sinh} &= 0.487644 - 0.00694171\beta^2_{sinh} \\ &= 0.487644 + 0.00694171\beta^2_{sin} \\ &\approx 0.488345 + 0.00814477\beta^2_{sin} \\ &= Z_{sin} \end{aligned}$$

8 Further Discussion and Conclusion

8.1 Comment on Results

I am very pleased with the results for the harmonic oscillator and the scalar field. The results from the Monte Carlo simulations agree very well with the predicted theoretical results and prove the worth of the method as a whole. The results for the Sinh-Gordon and Sin-Gordon fields were less conclusive, but appeared to indicate the relationships mentioned before. I am confident that if the calculations were averaged over a larger ensemble of configurations (perhaps 5000 instead of 2500) then the results[6] would become even more convincing. It was unfortunate that computer time was at a premium and this was not an option.

Of course the Sin-Gordon and Sinh-Gordon fields represent the tip of the iceberg. Whilst researching this project I have come across a huge variety of different directions that this project could have been taken in, with a little more time. Infact, there seems to be more than enough areas of study to write a whole PhD thesis on! This section of the paper aims to briefly introduce the reader to some of the relevant literature and comment on areas of interest that I would have liked to investigate further.

8.2 Relations and symmetry between different models

One of the most striking things that I have noticed during my research, is the vast amount of similarities and relations between different models and fields. For example, it is well known [4] that there is a duality between the quantum sine-Gordon (SG) and the massive Thirring (MT) models, where:

$$\begin{aligned} L^{SG} &= \frac{1}{2}(\partial_\mu \phi)^2 + \frac{\alpha}{\beta^2}[\cos(\beta\phi) - 1] \\ L^{MT} &= \bar{\mathrm{q}}(i\partial - m)\mathrm{q} - \frac{1}{2}g(\bar{\mathrm{q}}\ \gamma^\mu\ \mathrm{q})^2 \end{aligned}$$

which was first convincingly demonstrated by Coleman in 1974. However, [21] studied the mass spectrum of the Sine-Gordon model on a cylinder in the UV and IR regime and their results strongly confirm the conjecture of Klassen and Melzer that the sine-Gordon and massive Thirring models are *not* equivalent when defined on a *finite* cylinder.

In [9] they are interested in the Sinh-Gordon theory, where they choose to define the action by:

$$S = \int d^2x \left[\frac{1}{2}(\partial_\mu \phi)^2 - 2\frac{m^2}{g^2}\cosh(g\phi)\right]$$

The authors reminds us that it is the simplest example of an affine Toda Field Theory, possessing a Z_2 symmetry $\phi \to -\phi$ and that by means of an analytic continuation in g, i.e. $g \to ig$, it can be formally mapped to the Sine-Gordon model, as indicated by my own results.

[6] such as the match between m_{fit} and β^2

The authors go on to state that there are numerous alternative viewpoints for the Sinh-Gordon model. First, it can be regarded either as a perturbation of the free massless conformal action by means of a relevant operator $\cosh(g\phi)$. Alternatively, it can be considered as a perturbation of the conformal Liouville action:

$$S = \int d^2x \left[\frac{1}{2}(\partial_\mu \phi)^2 - \lambda e^{g\phi}\right]$$

by means of the relevant operator $e^{g\phi}$ or as a conformal A_1-Toda Theory, in which conformal symmetry is broken by setting the free field to zero. They continue, pointing out that the Sinh-Gordon model can be mapped into a Coulomb Gas System with an integer set of charges.

By means of an identity involving Bessel functions, in [9] the Euclidean partition function of this model is transformed into a form where it depends on the partition function of the massless theory and the two dimensional massless propagator.

[11] studies kink and kink lattice mechanics in the Double Sinh-Gordon model. Via scrutiny of the equation of motion identifies an important connection between the kink (and kink lattice) solutions of the ϕ^4 model and the double sine-Gordon (DSG) and DSHG models. Given a certain form of the ϕ^4 potential, the substitution $u = \tanh(\phi)$ or $u = \tan(\phi)$ leads to a DSGH model or a DSG model. This means that all known solutions (in that case) of the ϕ^4 equations of motion can be directly taken over to the DSHG and DSG equations of motion (and vice versa).

Dualities in more complex theories also exist. For example the conjectured duality between $G_2^{(1)}$ Affine Toda Field Theory and the $D_4^{(3)}$ theory is fully investigated using Monte Carlo techniques in [15].
A flow diagram in [22], by means of various limits and transformations, suggests further relations. The elliptic sine-Gordon model is related to the sine-Gordon model and the elliptic $D_{n+1}^{(1)}$-affina Toda theory, which is itself related to the minimal $D_{n+1}^{(1)}$-affina Toda theory and the free theory, whilst the sine-Gordon model is related to the free theory and the minimal $D_{n+1}^{(1)}$-affina Toda theory.

Clearly, there are many more relations and similarities between various theories and models, both already found in the literature, and I am sure, waiting to be found in the future. I am intrigued by these similarities, that remind me of the similarity between lattice field theories and thermodynamical systems, and would have liked to investigate this area further.

8.3 Correlation Functions from Form Factors

Another topic that seemed to continuously rear it's head during my research was the application of the theory of Form factors to finding correlation functions.

[1,6,9,20] imply that: The two-point correlation function for a hermitian operator O in real Euclidean space can be presented as an infinite series of form factors contributions:

$$< 0|O(0,0)O(x,t)|0 > = \sum_{n=0}^{\infty} \int \frac{d^n\beta}{n!(2\pi)^n} |F_n(d\beta_1, \cdots, d\beta_n)|^2 \prod_{j=1}^{n} e^{-mr\cosh(\beta_j)}$$

where r denotes the radial distance $r = \sqrt{x_1^2 + x_2^2}$ and θ is the rapidity that is related to the momentum via $p_i = m_i \sinh(\beta_j)$. All integrals are convergent and one expects a convergent series as well. Similar expressions can be derived for multi-point correlators.

[1] goes on to use the Fredholm determinant representation for derivation of the asymptotic behaviour of the sinh-Gordon correlation function, to find:

$$< 0|O(0,0)O(x,t)|0 > \rightarrow \frac{|H_0|^2}{|s^2|} + |H_1|^2 \ (2\pi mr)^{-1/2} e^{-mr} \quad (5.14) \text{ in } [1]$$

The author of [1] then remind us that for a correlation function of local fields one should put $H_0 = 0 = \frac{H_0}{[s]}$, so that the asymptotic formula above is well defined for arbitrary s. Formula (1.13) in [1] gives us $H_0 = < 0|\phi(0)|0 > = 0$ and $H_1 = < 0|\phi(0)|\beta > = \frac{1}{\sqrt{2}}$. So combining these seemed to imply that the correlation function would be of the form: $\frac{1}{2\sqrt{2\pi m}} \frac{e^{-mr}}{\sqrt{r}}$ which is the same form as I expected for the scalar field.

A fit of this kind to the Sinh-Gordon data was seeked by the process of least square minimisation with some success in the course of this paper. However the fit was poor to the Sin-Gordon data, and the fits didn't indicate any relations between the Sin-Gordon and Sinh-Gordon data, as was found in section 7. This was a little perplexing, but I know little on the topic of Form Factors and with further research and more time I would have liked to investigate whether some agreement between theory and simulation could have been found.

8.4 S-Matrices

In [8], using the action previously stated, it is stated that the two particle sine-Gordon S-matrix for the scattering of fundamental bosons (lowest breathers) is:

$$S(\theta) = \frac{\sinh(\theta) + i\sin(\pi\nu)}{\sinh(\theta) - i\sin(\pi\nu)}$$

where θ is the rapidity difference defined by $p_1 p_2 = m^2 \cosh(\theta)$ and ν is related to the coupling constant by $\nu = \frac{\beta^2}{8\pi - \beta^2}$.

In [9] the Sinh-Gordon model with the following action is considered:

$$S = \int d^2x \left[\frac{1}{2}(\partial_\mu\phi)^2 - 2\frac{m^2}{g^2}\cosh(g\phi)\right]$$

The two particle S-matrix for the Sinh-Gordon theory is then stated to be given by:

$$S(\beta, B) = \frac{\tanh(\frac{\beta}{2} - i\frac{\pi B}{4})}{\tanh(\frac{\beta}{2} + i\frac{\pi B}{4})}$$

where B is the following function of the coupling constant g: $B(g) = \frac{2g^2}{8\pi+g^2}$.

S-Matrices are a rich topic to be researched in their own right [14,15], and I would have liked to explore the topic more thoroughly as I had barely begun to scratch the surface with my own reading.

8.5 Wave function Renormalization

In [4] the finite sine-Gordon wave function renormalization constant is determined exactly. The paper utilises the same action as in this paper:

$$L^{SG} = \frac{1}{2}(\partial_\mu\phi)^2 + \frac{\alpha}{\beta^2}[\cos(\beta\phi) - 1]$$

The purpose of having $\cos(\beta\phi) - 1$ in the potential as opposed to simply $\cos(\beta\phi)$ is so that the potential is equal to zero[7] when $\phi = 0$.

In [4] Weisz determines exactly the Sine-Gordon wavefunction renomalization constant, defined on $\lambda > 1$ by $< 0|\phi(0)|b_1 > = \sqrt{Z(\lambda)}$, where $\lambda = \frac{8\pi}{\beta^2} - 1$, or

$$< \phi(x)\phi(y) > = Z(\lambda)\Delta_+(x - y, m_1^2) + \text{contributions from larger masses}$$

After some calculation he concludes that:

$$Z(\lambda) = \left(1 + \frac{1}{\lambda}\right)\left(\frac{2\lambda}{\pi}\sin\left[\frac{\pi}{2\lambda}\right]\right)^{-1} \exp\left[-\frac{1}{\pi}\int_0^{\pi/\lambda} dx \frac{x}{\sin(x)}\right]$$

and for $\lambda \to \infty$, which corresponds to $\beta \to 0$, the SG theory becomes free and :

$$Z\left(\frac{8\pi}{\beta^2} - 1\right) = 1 - \left(\frac{\beta^2}{8\pi}\right)^2\left(\frac{1}{2} - \frac{1}{24}\pi^2\right) + O(\beta^6)$$

For arbitrary λ with $1 \leq \lambda \leq \infty$, i.e. $0 \leq \beta^2 \leq 4\pi$, we have $0 \leq Z(\lambda) \leq 1$ which is a general consequence of positivity. The Z in my simulation were indeed found to obey the property $0 \leq Z \leq 1$, but were in poor agreement with

[7] This is analogous to having $1 - \cosh(\beta\phi)$ in the potential for the Sinh-Gordon model as opposed to $\cosh(\beta\phi)$.

this formula. I would think that this is because, in my simulation, the smallest β used is $\beta = \frac{1}{4}$ which corresponds to $\lambda \approx 400$, and the relation above holds for $\lambda \to \infty$, so perhaps I should have investigated smaller values of β. Better agreement between theory and prediction was expected.

From [4] a simple transformation $\nu = 1/\lambda$ gives the result from [8]:

$$< 0|\phi(0)|p > = \sqrt{Z} \text{ with } Z = (1+\nu)\frac{\frac{\pi}{2}\nu}{\sin[\frac{\pi}{2}\nu]} \exp\left[-\frac{1}{\pi}\int_0^{\pi\nu} \frac{t}{\sin(t)}dt\right]$$

which is the normalization of a fundamental bose field annihiliating a one-particle state, where $Z = 1 + O(\beta^4)$ is the wave function renormalization constant calculated in [4]. This gives the normalisation constant $N_1^{(1)} = \frac{\sqrt{Z}}{2}$ for the form factors of the fundamental bose field.

In [2] another expression (formula 4.38) for the wavefunction renormalization constant Z is given:

$$Z(B) = \frac{\pi B(2-B)}{8\sin[\frac{\pi B}{4}]} \exp\left[-\frac{1}{\pi}\int_0^{-\frac{\pi B}{2}} dz \frac{z}{\sin(z)}\right]$$

where $B = -\frac{2}{\lambda}$ (and once again $\lambda = \frac{8\pi}{\beta^2} - 1$) makes it conincide exactly with the result from [4].

The values of Z that were found during my simulation did not agree with these formulae from the literature. I believe the non-agreement is due to the fact that all my simulations had a lattice spacing $a = 1$. In the limit $a \to 0$ the results from simulation should approach the theoretical predictions of these formulae. This is something I would have liked to investigate further.

8.6 Mass Renormalization

This is another topic that consistently appeared in the literature during my research, but that I didn't have time to pursue as fully as I would have liked. In [8,18] it has been found that the quantum sine-Gordon field equations hold with an exact relation between the "bare" mass and the renormalized mass.

$$L^{SG} = \frac{1}{2}(\partial_\mu\phi)^2 + \frac{\alpha}{\beta^2}[\cos(\beta\phi) - 1]$$

is the action being considered, and if ν is related to the coupling constant by $\nu = \frac{\beta^2}{8\pi-\beta^2}$, then the "bare" mass $\sqrt{\alpha}$ is related to the renormalized mass by $\alpha = m^2\frac{\pi\nu}{\sin(\pi\nu)}$ where m is the physical mass of the fundamental boson. The factor $\frac{\pi\nu}{\sin(\pi\nu)}$ has to be considered as a quantum correction to the classical equation.

Note, in particular at the "free fermion point" $\nu \to 1$ or $\beta^2 \to 4\pi$, this factor diverges, a phenomenon which is to be expected by short distance investigations. For fixed bare mass square α and $\nu \to 2, 3, 4, \cdots$ the physical mass goes to zero.

The authors go on to state that in lowest order the relation between the bare and the renormalized mass α is given by:

$$m^2 \;=\; \left[1 - \frac{1}{6}\left(\frac{\beta^2}{8}\right)^2 \;+\; O(\beta^6)\right]$$

Other papers [7,19] use the slightly different euclidean action for the sine-Gordon model:

$$S \;=\; \int d^2x \left[\frac{1}{16\pi}(\partial_\mu \phi)^2 - 2\mu\cos(\beta\phi)\right]$$

This is invariant w.r.t. the field translations $\phi(x) \rightarrow \phi(x) \;\pm \frac{2\pi}{\beta}$ where ϕ is a real Bose field. The spectrum of this model includes the soliton, anti-soliton and some number (depending on the coupling constant g) of their bound states names breathers.

[19] goes on to give an exact relation between the soliton mass M and the parameter μ in the action:

$$\mu \;=\; \frac{\Gamma(\beta^2)}{\pi\Gamma(1-\beta^2)}\left[\frac{M\sqrt{\pi}\Gamma\left(\frac{1+\xi}{2}\right)}{2\Gamma\left(\frac{\xi}{2}\right)}\right]^{2-2\beta^2}$$

where $\xi \;=\; \frac{\beta^2}{1-\beta^2}$.

I briefly attempted to find correlation between the masses found in my Sine-Gordon simulations and those predicted by these theories, again with little success. The study of breathers (or kinks), solitons and instantons in the Sine-Gordon model is widespread, for example in [10] breather form factors are calculated starting with the general formula for the soliton form factors.

8.7 Conclusion

I hope this paper has served to show the validity of the Monte Carlo approach to investigation of quantum field theories. With the limited processing power of my home computer, only the simplest of scenarios could be considered. Where the method comes into it's own is in the investigation of a field known as Quantum Chromodynamics. Here a hypercubic space-time lattice is used, where quarks are defined at lattice sites and gluons are defined by eight dimensional integrals on the links between lattice sites. More sophisticated updating algorithms are used, and the fine tuning of the simulation to deal with systematic discretization errors is a mammoth task. Clearly, that is beyond the scope of this paper.

9 Appendix A - Graphs

9.1 One Dimensional Harmonic Oscillator

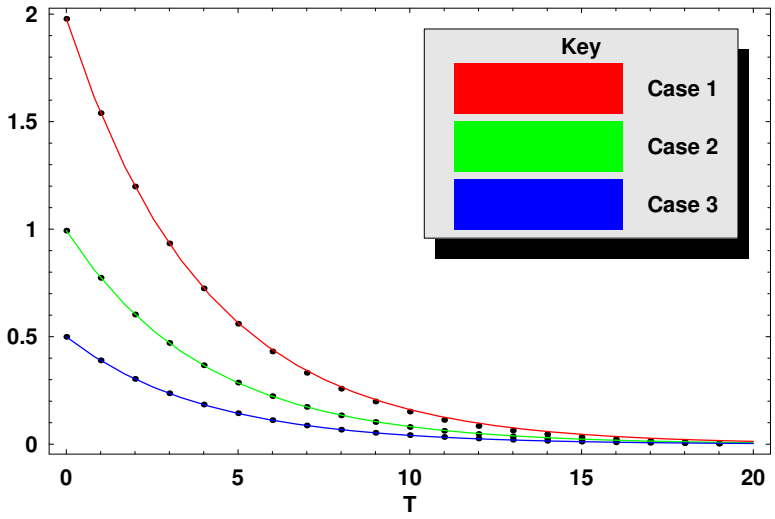

Figure 5: Leading Behaviour of $< \phi(0)\phi(T) >$ for $am = 0.25$

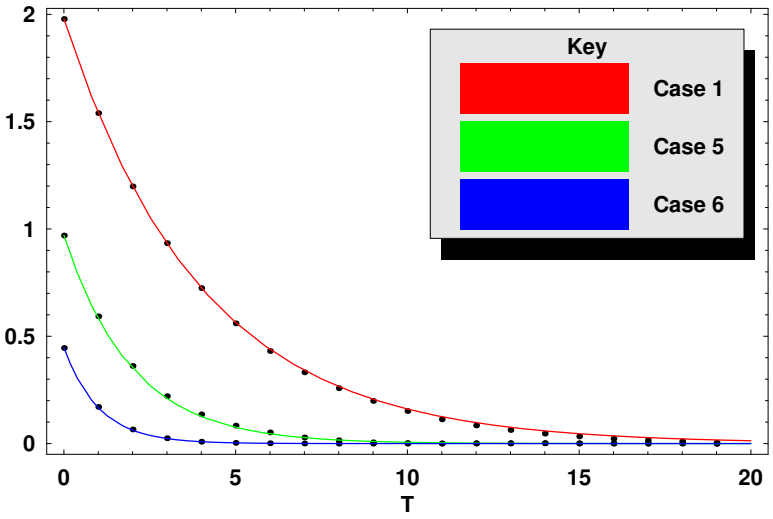

Figure 6: Leading Behaviour of $< \phi(0)\phi(T) >$ for $a = 1$

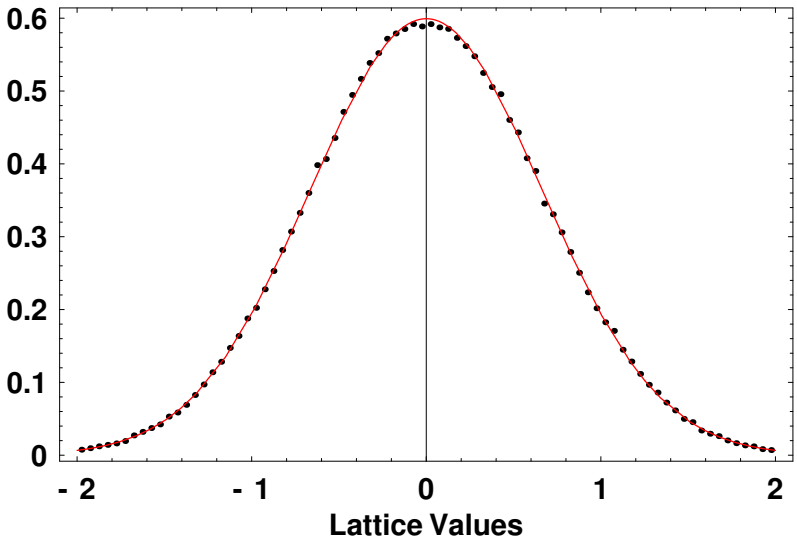

Figure 7: Probability Distribution of Lattice Site values.

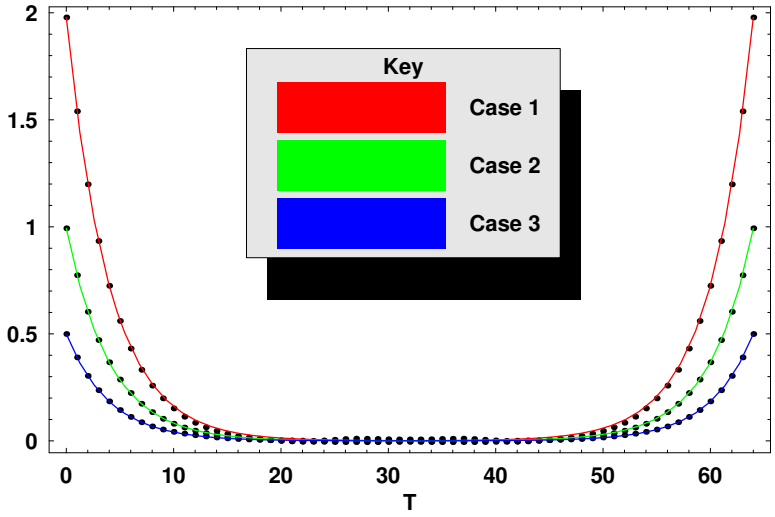

Figure 8: Plot of the whole Correlation Function $< \phi(0)\phi(T) >$ for $am = 0.25$

The graph above is shown as an example of how one can find a fit to the entire correlation function across the whole lattice, in this case 64 sites. The rest of the graphs in this Appendix will be of the form of Figure 1 and Figure 2 showing only the leading behaviour as this is what we are interested in.

9.2 Two Dimensional Free Scalar Field

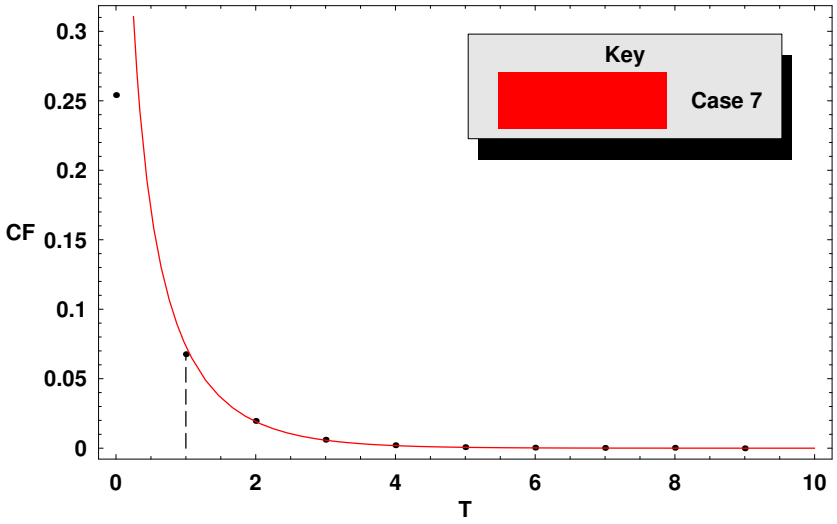

Figure 9: Long Distance Behaviour of $< \phi(0)\phi(T) >$ for Case 7.

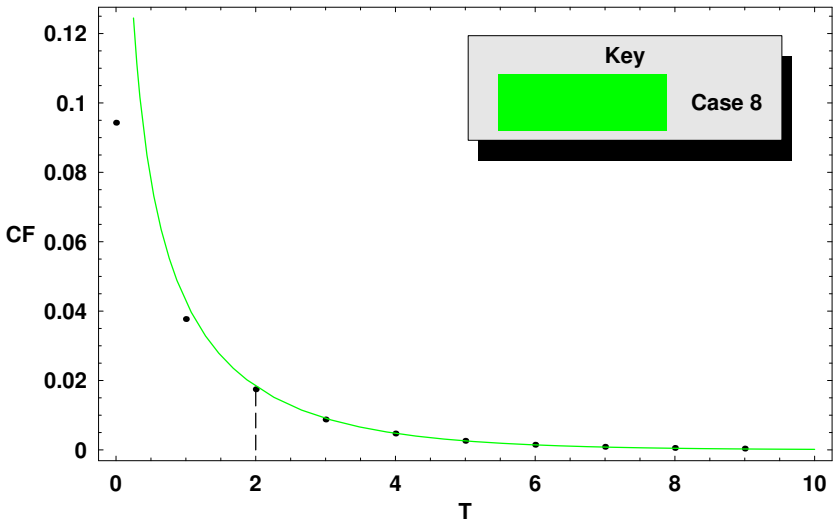

Figure 10: Long Distance Behaviour of $< \phi(0)\phi(T) >$ for Case 8.

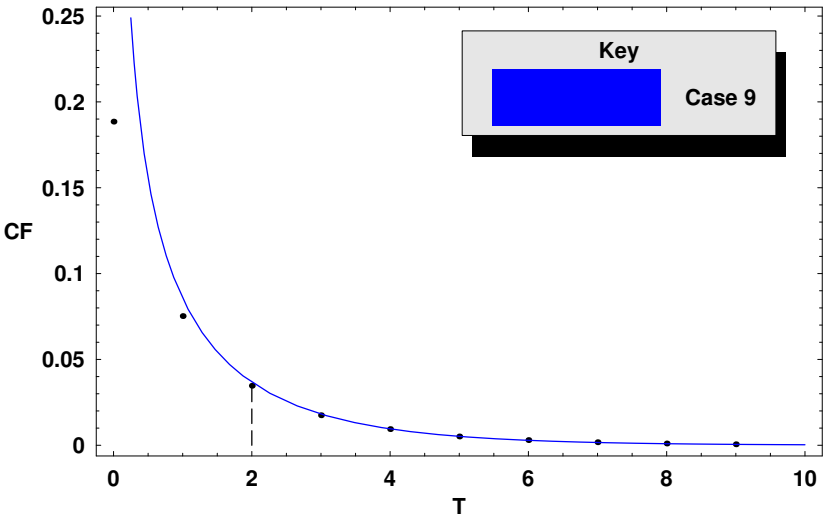

Figure 11: Long Distance Behaviour of $< \phi(0)\phi(T) >$ for Case 9.

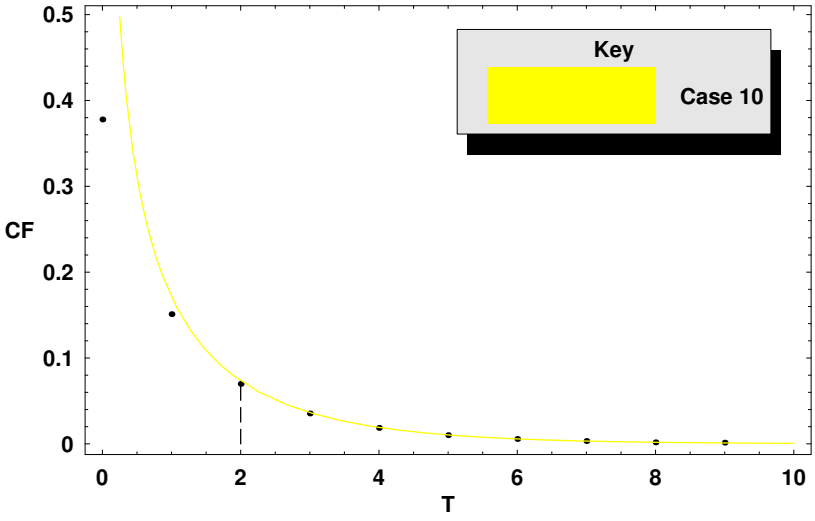

Figure 12: Long Distance Behaviour of $< \phi(0)\phi(T) >$ for Case 10.

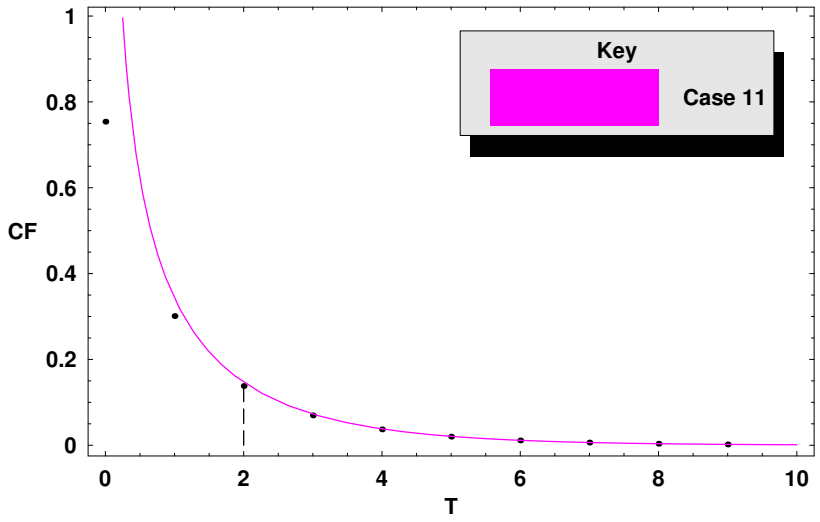

Figure 13: Long Distance Behaviour of $< \phi(0)\phi(T) >$ for Case 11.

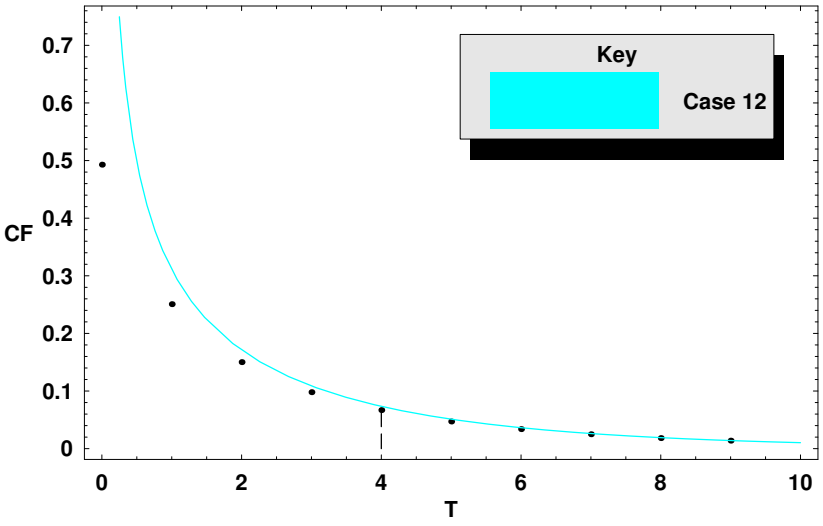

Figure 14: Long Distance Behaviour of $< \phi(0)\phi(T) >$ for Case 12.

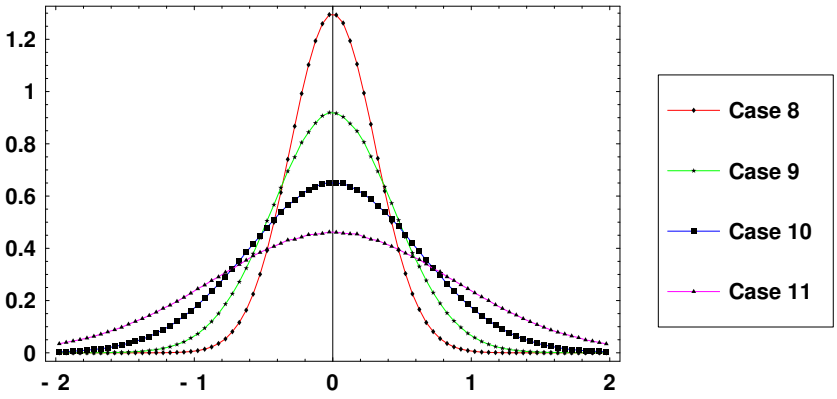

Figure 15: Probability Distribution for $am = \frac{1}{2}$.

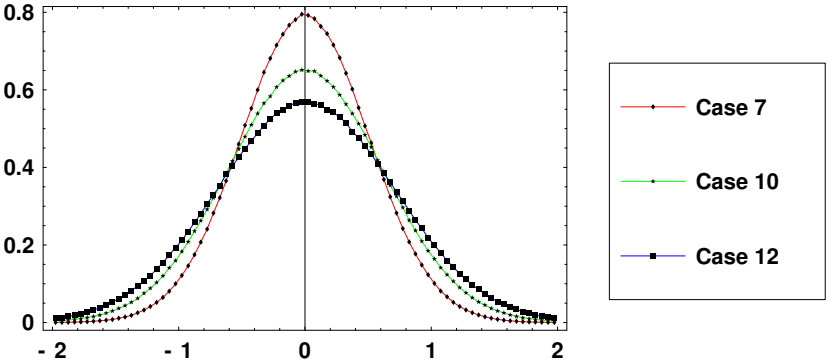

Figure 16: Probability Distribution for $a = 1$.

9.3 Two Dimensional Sinh-Gordon Field

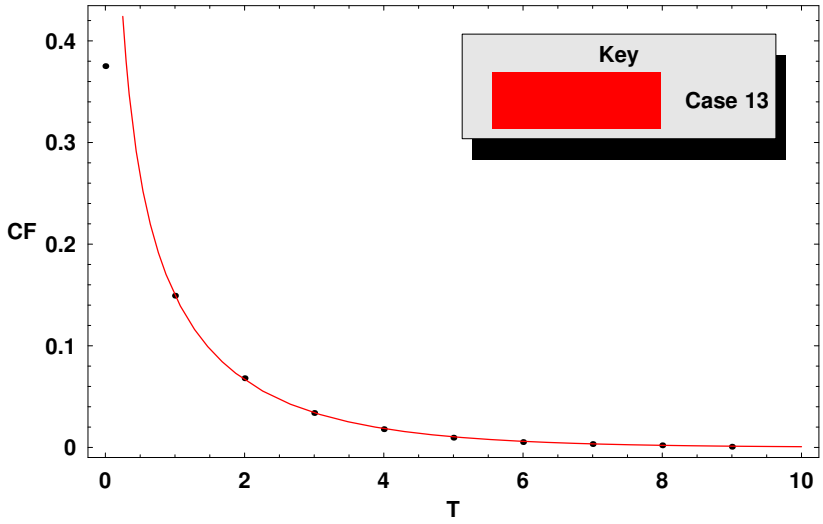

Figure 17: Long Distance Behaviour of $< \phi(0)\phi(T) >$ for Case 13.

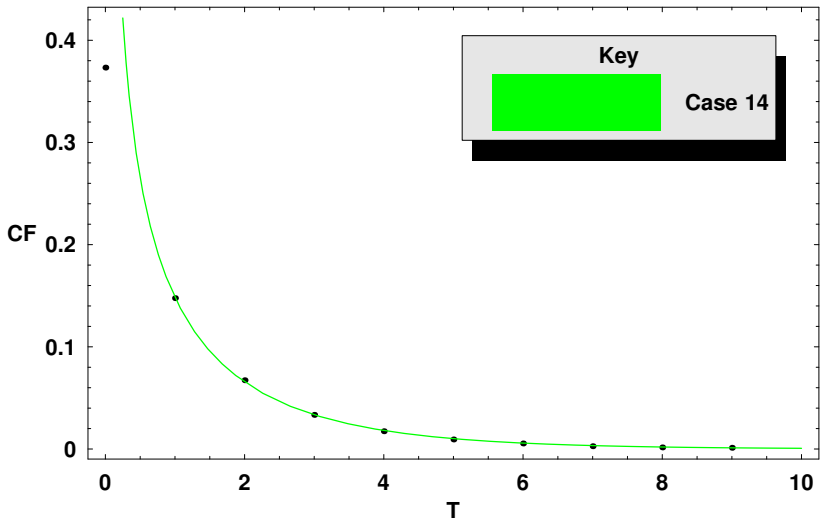

Figure 18: Long Distance Behaviour of $< \phi(0)\phi(T) >$ for Case 14.

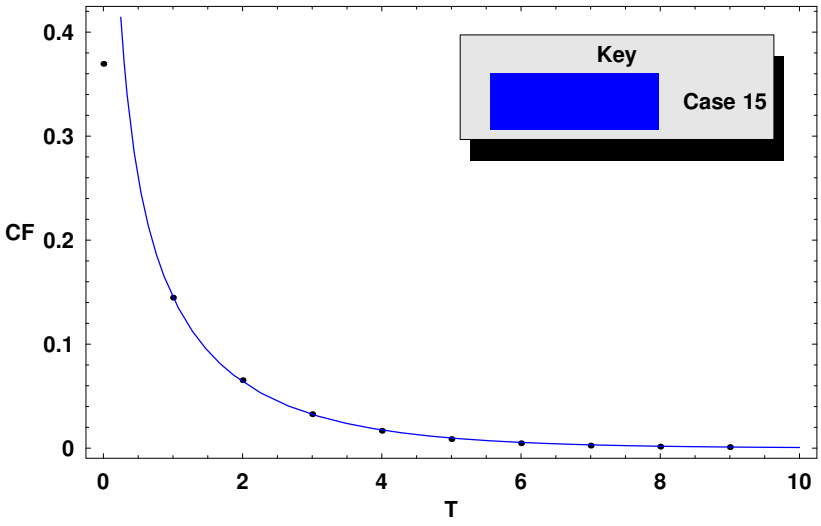

Figure 19: Long Distance Behaviour of $< \phi(0)\phi(T) >$ for Case 15.

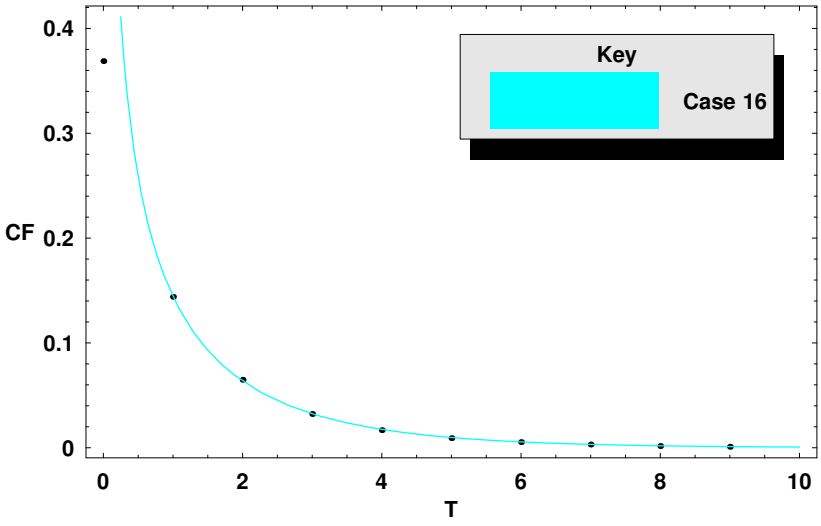

Figure 20: Long Distance Behaviour of $< \phi(0)\phi(T) >$ for Case 16.

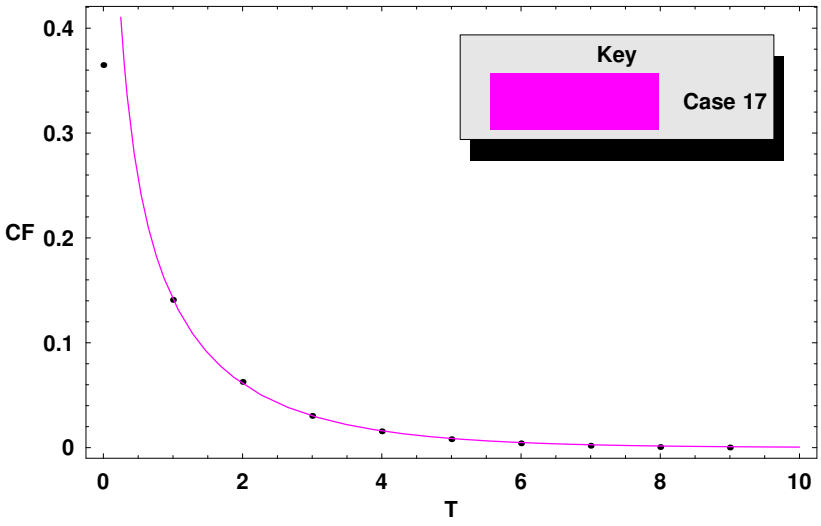

Figure 21: Long Distance Behaviour of $< \phi(0)\phi(T) >$ for Case 17.

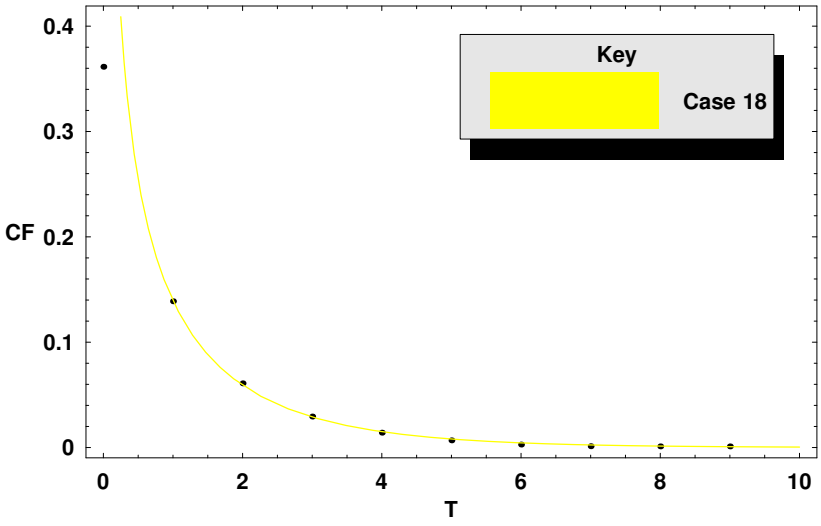

Figure 22: Long Distance Behaviour of $< \phi(0)\phi(T) >$ for Case 18.

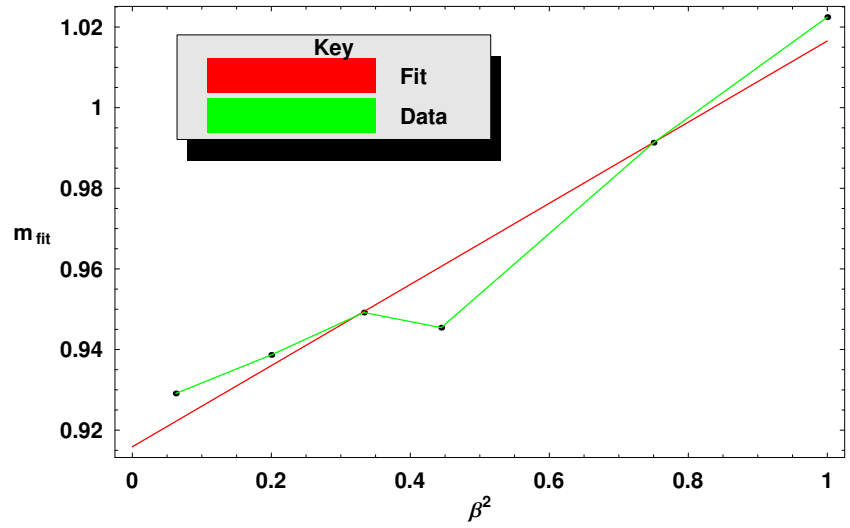

Figure 23: A plot of m_{fit} against β^2.

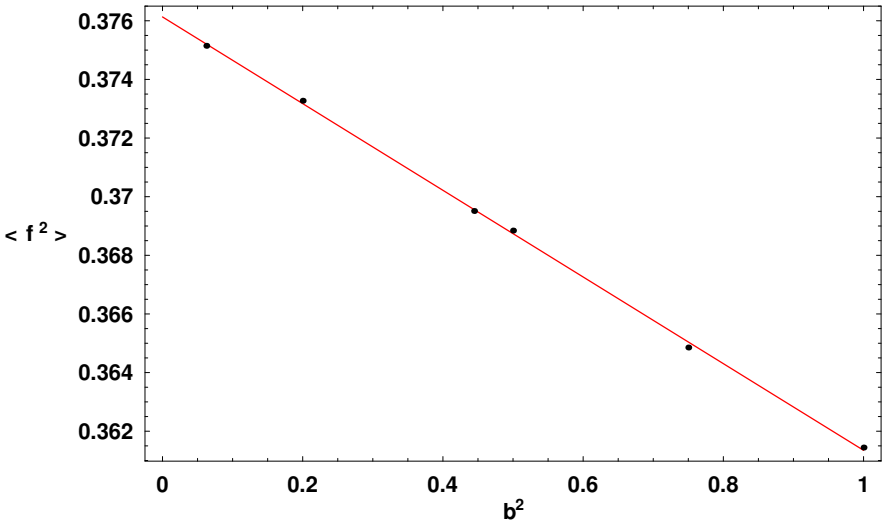

Figure 24: A plot of $< \phi(0)^2 >$ against β^2.

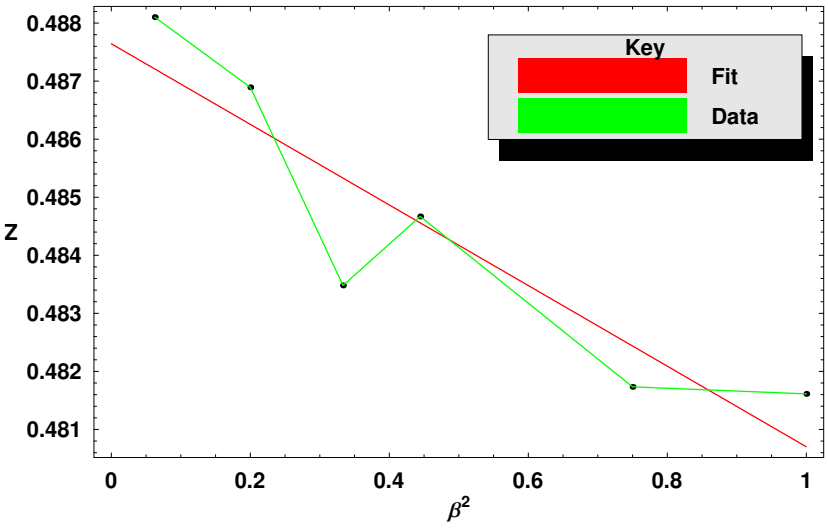

Figure 25: A plot of Z against β^2.

9.4 Two Dimensional Sin-Gordon Field

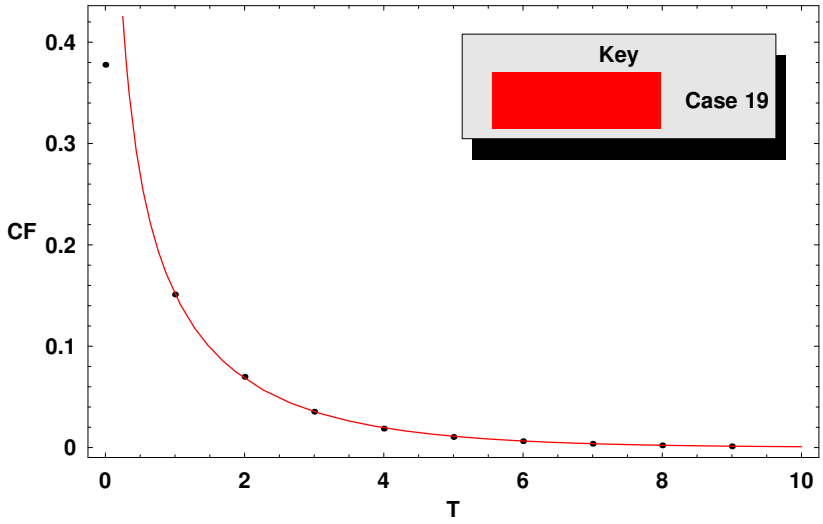

Figure 26: Long Distance Behaviour of $< \phi(0)\phi(T) >$ for Case 19.

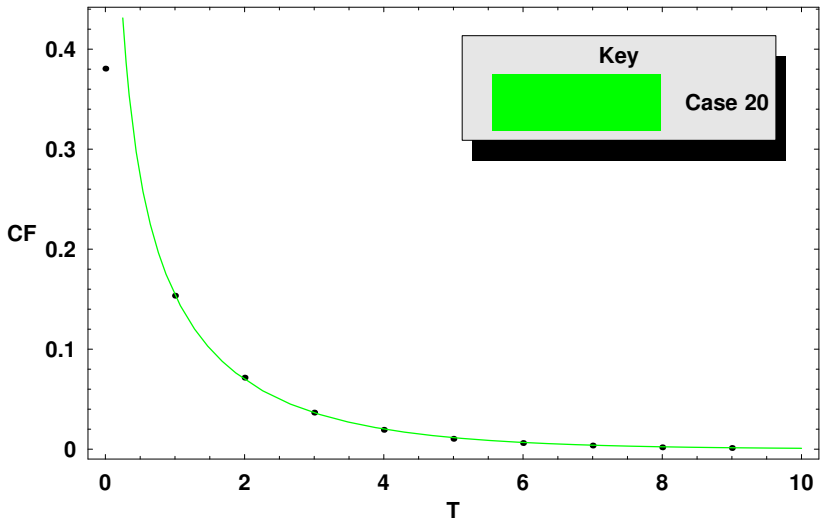

Figure 27: Long Distance Behaviour of $< \phi(0)\phi(T) >$ for Case 20.

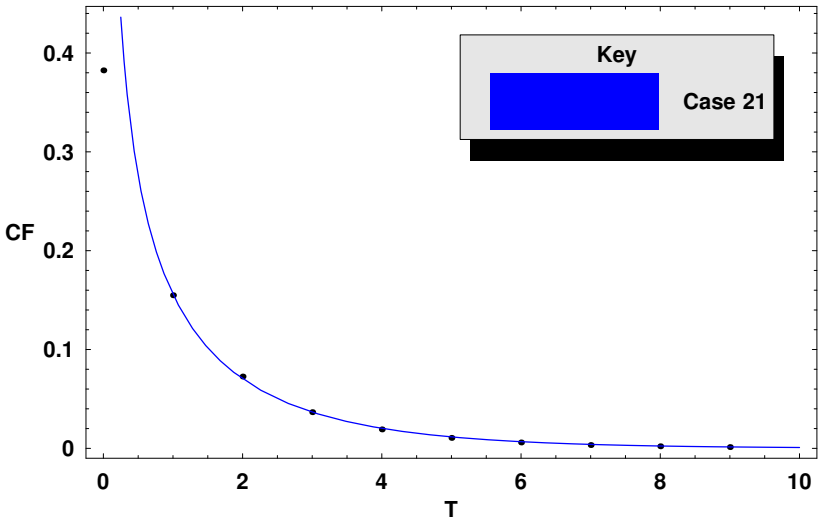

Figure 28: Long Distance Behaviour of $< \phi(0)\phi(T) >$ for Case 21.

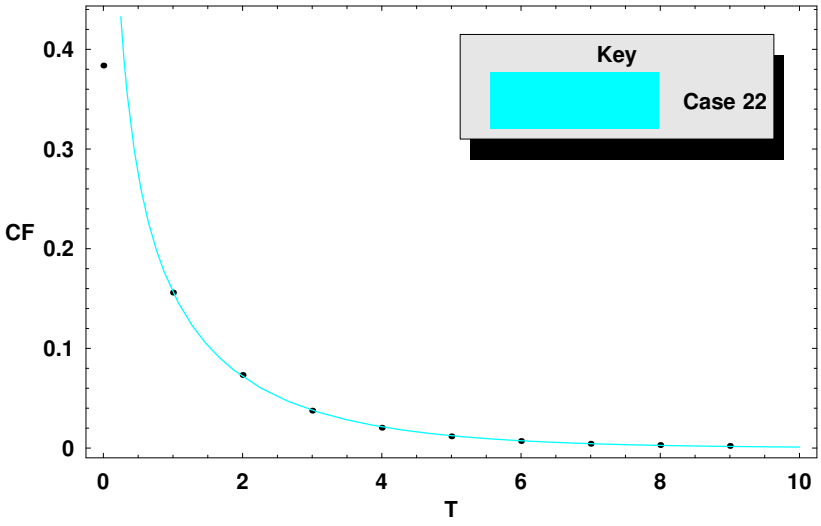

Figure 29: Long Distance Behaviour of $< \phi(0)\phi(T) >$ for Case 22.

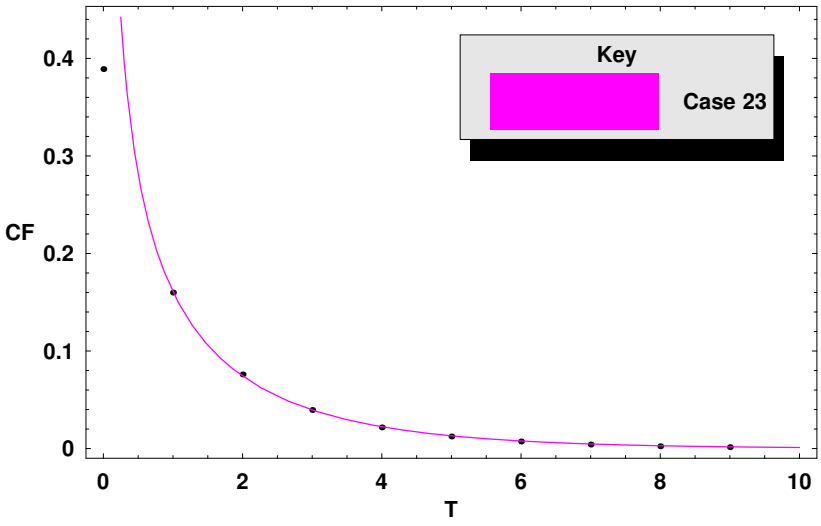

Figure 30: Long Distance Behaviour of $< \phi(0)\phi(T) >$ for Case 23.

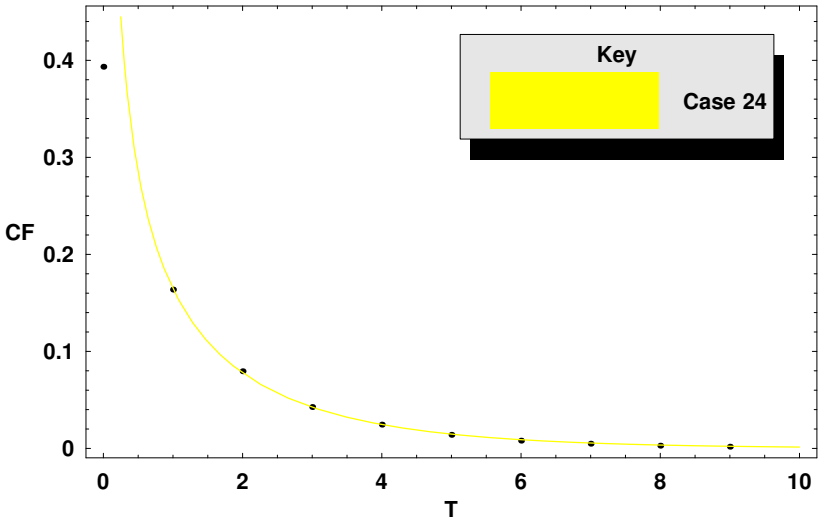

Figure 31: Long Distance Behaviour of $< \phi(0)\phi(T) >$ for Case 24.

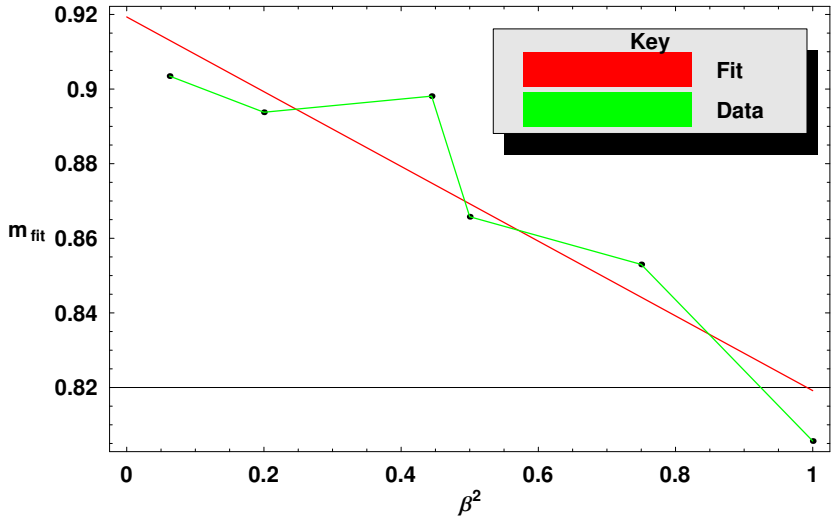

Figure 32: A plot of m_{fit} against β^2.

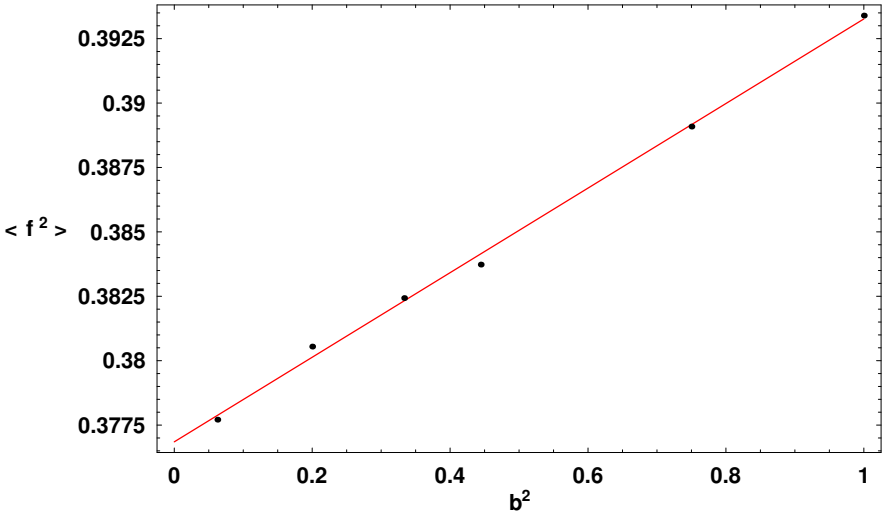

Figure 33: A plot of $<\phi(0)^2>$ against β^2.

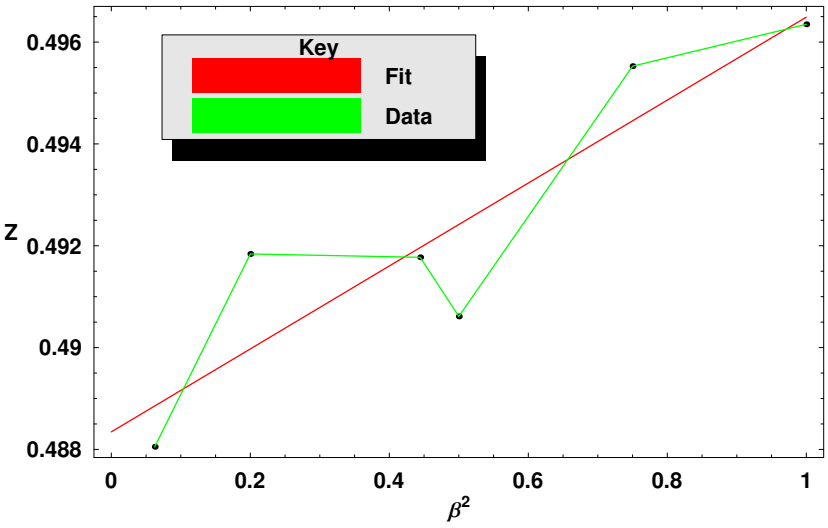

Figure 34: A plot of Z against β^2.

10 Appendix B - Tables

Throughout this section the following conventions hold:

- a is the lattice spacing as it appears in the discrete lattice action.
- m is the mass parameter as it appears in the discrete lattice action.
- β is an extra parameter that appears in the actions for the Sinh-Gordon and Sin-Gordon fields only.
- M is the length of the lattice, corresponding to the number of discrete time steps.
- σ is the standard deviation of the normal distribution which the random numbers are chosen from.
- ε is the number of lattice sweeps ignored between calculations.
- $< x^2 >_D$ is the discrete expectation value of x^2 as calculated in sections 3.5 and 4.4.
- For the simple harmonic oscillator, m_{fit} is the m from the $\frac{1}{2m}e^{-mx}$ fit to the simulation correlation function calculated during the simulation.
- For the free scalar field, m_{fit} is the m from the $\frac{1}{2\sqrt{2m}}\frac{e^{-mx}}{\sqrt{x}}$ fit to the long distance behaviour of the simulation correlation function calculated during the simulation.
- For the Sin-Gordon and Sinh-Gordon fields, m_{fit} and Z are as they appear in the $Z^2\frac{e^{-m(m_{fit})x}}{\sqrt{x}}$ fit to the long distance behaviour of the simulation correlation function calculated during the simulation by the process of least square minimisation.
- $< x^2 >_{fit}$ is the average value of x^2, averaged across all lattice sites and all lattices in a particular case. In relation to the correlation function, it is given by $< \phi(0)^2 >$.

10.1 One Dimensional Harmonic Oscillator

Simulation Parameters						
Case	a	m	M	σ	Acceptance Rate	ε
1	1.00	0.25	64	1.40	49.6796%	200
2	0.50	0.50	64	1.00	49.5541%	200
3	0.25	1.00	64	0.70	49.8902%	200
4	0.50	1.00	64	0.95	49.7535%	100
5	1.00	0.50	64	1.30	50.7090%	100
6	1.00	1.00	64	1.15	50.2543%	50

Simulation Results						
Case	a	m	am	m_{fit}	$< x^2 >_D$	$< x^2 >_{fit}$
1	1.00	0.25	0.25	0.250938	1.984561	1.978293
2	0.50	0.50	0.25	0.249665	0.992278	0.993108
3	0.25	1.00	0.25	0.250095	0.496139	0.499263
4	0.50	1.00	0.50	0.499702	0.485701	0.484769
5	1.00	0.50	0.50	0.509858	0.970143	0.969370
6	1.00	1.00	1.00	0.984252	0.447214	0.445382

10.2 Two Dimensional Scalar Free Field

Simulation Parameters						
Case	a	m	M	σ	Acceptance Rate	ε
7	1.00	1.00	32	0.90	49.8075%	50
8	0.25	2.00	32	0.49	49.6744%	100
9	0.50	1.00	32	0.68	50.2764%	100
10	1.00	0.50	32	0.95	50.6501%	100
11	2.00	0.25	32	1.35	50.5265%	100
12	1.00	0.25	32	1.00	49.7313%	200

Simulation Results						
Case	a	m	am	m_{fit}	$< x^2 >_D$	$< x^2 >_{fit}$
7	1.00	1.00	1.00	0.999702	0.254050	0.254101
8	0.25	2.00	0.50	0.502317	0.0942138	0.0943046
9	0.50	1.00	0.50	0.510632	0.188428	0.188510
10	1.00	0.50	0.50	0.498932	0.376855	0.377874
11	2.00	0.25	0.50	0.506295	0.753711	0.753927
12	1.00	0.25	0.25	0.256921	0.493300	0.492872

10.3 Sinh-Gordon Field and Sin-Gordon Field

Sinh-Gordon Simulation Parameters						
Case	β	a	M	σ	Acceptance Rate	ε
13	$1/4$	1.00	32	0.95	50.6749%	100
14	$1/\sqrt{5}$	1.00	32	0.95	50.6618%	100
15	$1/\sqrt{3}$	1.00	32	0.95	50.5953%	100
16	$2/3$	1.00	32	0.95	50.6191%	100
17	$\sqrt{3}/2$	1.00	32	0.95	50.5842%	100
18	1	1.00	32	0.95	50.8143%	100

Sinh-Gordon Simulation Results						
Case	β	m	β^2	Z	m_{fit}	$< x^2 >_{fit}$
13	$1/4$	0.50	$1/16$	0.488102	0.929103	0.375146
14	$1/\sqrt{5}$	0.50	$1/5$	0.486893	0.938673	0.373273
15	$1/\sqrt{3}$	0.50	$1/3$	0.483481	0.949182	0.369512
16	$2/3$	0.50	$4/9$	0.484669	0.945426	0.368844
17	$\sqrt{3}/2$	0.50	$3/4$	0.481734	0.991326	0.364855
18	1	0.50	1	0.481613	1.022455	0.361443

Sin-Gordon Simulation Parameters						
Case	β	a	M	σ	Acceptance Rate	ε
19	$1/4$	1.00	32	0.95	50.6749%	100
20	$1/\sqrt{5}$	1.00	32	0.95	50.6618%	100
21	$2/3$	1.00	32	0.95	50.5953%	100
22	$1/\sqrt{2}$	1.00	32	0.95	50.6191%	100
23	$\sqrt{3}/2$	1.00	32	0.95	50.5842%	100
24	1	1.00	32	0.95	50.8143%	100

Sin-Gordon Simulation Results						
Case	β	m	β^2	Z	m_{fit}	$< x^2 >_{fit}$
19	$1/4$	0.50	$1/16$	0.488502	0.903478	0.377710
20	$1/\sqrt{5}$	0.50	$1/5$	0.491839	0.893782	0.380548
21	$2/3$	0.50	$4/9$	0.491773	0.898104	0.382430
22	$1/\sqrt{2}$	0.50	$1/2$	0.490612	0.865773	0.383731
23	$\sqrt{3}/2$	0.50	$3/4$	0.495527	0.852991	0.389088
24	1	0.50	1	0.496349	0.805654	0.393396

11 References

1. *The determinant representation for quantum correlation functions of the sinh-gordon model*
   by V. Korepin and N. Slavnov
   J. Phys. A: Math Gen 31 (1998) 9283-9295.

2. *New Exact Results in Affine Toda Field Theories*
   by Destri and Vega
   Nuc. Phy. B358 (1991) 251-294.

3. *Exact Quantum Sine-Gordon Soliton Form Factors*
   by P. Weisz
   Phys. Lett. B67 (1977) 179-189.

4. *Exact Form Factors in (1+1)-Dimensional Field Theoretic Models with Soliton Behaviour*
   by P. Weisz
   Nuc. Phy. B139 (1978) 455-476.

5. *Form Factors in Sin(h)-Gordon theory*
   by A. Rosly and K. Slivanov
   Phys. Lett. B426 (1998) 334-338.

6. *Exact Form Factors in Integrable Quantum Field Theories: the Sine-Gordon Model*
   by H Babujian, A. Fring, M Karowski and A. Zapletal
   Nuc. Phys. B538 (1999) 535-586.

7. *Form Factors of soliton-creating operators in the sine-Gordon Model*
   by S. Lukyanov and A Zamolodchikov
   Nuc. Phys. B607 (2001) 437-455.

8. *The Exact Quantum Sine-Gordon Field Equation and Other Non-Perturbative Results*
   by H. Babujian and M. Karowski
   Phys. Lett. B471 (1999) 53-57.

9. *Form Factors for Integrable Lagrangian Field Theories, the Sinh-Gordon Model*
   by A. Fring, G. Mussardo and P. Simonetti
   Nuc. Phys. B393 (1993) 413-441.

10. *Exact Form Factors in integrable Quantum Field Theories: the sine-Gordon Model (II)*
    by H. Babujian and M. Karowski
    Nuc. Phys. B620 (2002) 407-455.

11. *Statistical Mechanics of double sinh-Gordon kinks*
    by S.Habib, A. Khare and A. Saxena
    Physica D123 (1998) 341-356.

12. *Exact Results in the Statistical Mechanics of Integrable Models in (1+1) Dimensions*
by R. Bullough, D. Pilling and Yu-zhong Chen
JYFL-9-91, Jun 1990. 21pp.

13. *The simple harmonic oscillator ground state using a variational Monte Carlo method*
by S. Pottorf, A. Pudzer, M. Y. Chou and J. Hasbun
Eur. J. Phys. 20 (1999) 205-212.

14. *Monte Carlo study of exact S-matrix duality in non simply laced affine Toda theories*
by M. Beccaria
Phys. Rev. D53 (1996) 3266-3271.

15. G_2^1 *Affine Toda Field Theory: A Numerical Test of Exact S-Matrix results*
by G. Watts and R. Weston
Phys. Lett. B289 (1992) 61-66.

16. *Cost of the Generalised Hybrid Monte Carlo Algorithm for Free Field Theory*
by A. Kennedy an B. Pendleton
Nucl. Phys. B607 (2001) 456-510.

17. *The Euclidean Propagator in Quantum Models with Non-Equivalent Instantons*
by J. Casahorran
Proceedings of the Fourth International Conference about Symmetry in Nonlinear Mathematical Physics, Kiev, 2001.

18. *Sine-Gordon breather form factors and quantum field equations*
by H. Babujian and M. Karowski
J. Phys. A35 (2002) 9081-9104.

19. *Perturbation theory in radial quantization approach and the expectation values of exponential fields in sine-Gordon model*
by V. Mkhitaryan, R. Poghossian and T. Sedrakyan
J. Phys. A33 (2000) 3335-3346.

20. *The Form Factors in the Sinh-Gordon Model*
by M. Pillin
J. Mod. Phys. A13 (1998) 4469-4486.

21. *UV and IR Analyses of the Mass Spectrum in the Sine-Gordon Model*
by S. Pallua and P. Prester
FIZIKA B1 (Zagreb) 10 (2001) 175-186.

22. *Breathers in the elliptic sine-Gordon model*
by O. Castro-Alvaredo and A. Fring
J. Phys. A: Math Gen 36 (2003) 10233-10249.

23. *Introduction to Monte Carlo Methods*
by S. Weinzierl
Topical lectures given at the Research School Subatomic Physics, Amsterdam, June 2000.

24. *The Monte Carlo Method*
by Shreider
Pergamon Press.

25. *Monte Carlo Concepts, Algorithms, and Applications*
by Fishman
Springer.

26. *Monte Carlo Simulation in Statistical Physics*
by Binder and Heermann
Springer.

27. *Introduction to Quantum Fields on a Lattice*
by Smit
Cambridge Lecture Notes in Physics.

28. *Quantum Fields on a Lattice*
by Montvay and Munster
Cambridge Monographs on Mathematical Physics.